05 Jan 2024

Hanford Low-Activity Waste Vitrification: A Review

José Marcial

Brian J. Riley

Albert A. Kruger

Charmayne E. Lonergan
Missouri University of Science and Technology, clonergan@mst.edu

et. al. For a complete list of authors, see https://scholarsmine.mst.edu/matsci_eng_facwork/3261

Recommended Citation

J. Marcial et al., "Hanford Low-Activity Waste Vitrification: A Review," *Journal of Hazardous Materials*, vol. 461, article no. 132437, Elsevier, Jan 2024.
The definitive version is available at https://doi.org/10.1016/j.jhazmat.2023.132437

Journal of Hazardous Materials 461 (2024) 132437

Contents lists available at ScienceDirect

Journal of Hazardous Materials

journal homepage: www.elsevier.com/locate/jhazmat

Review

Hanford low-activity waste vitrification: A review

José Marcial [a], Brian J. Riley [a], Albert A. Kruger [b], Charmayne E. Lonergan [a,c], John D. Vienna [a,*]

[a] Nuclear Sciences Division, Pacific Northwest National Laboratory, Richland, WA 99354, USA
[b] US Department of Energy, Office of River Protection, Richland, WA 99352, USA
[c] Materials Science and Engineering, Missouri University of Science and Technology, Rolla, MO 65409

HIGHLIGHTS

- The worlds largest nuclear waste treatment plant is starting operation in 2024.
- Over 20 years of effort has led to the technology to treat the mixed hazardous-radioactive waste stored in Hanford tanks.
- This review summarizes over 230 documents that tell the story of technology development and optimization for the plant.

GRAPHICAL ABSTRACT

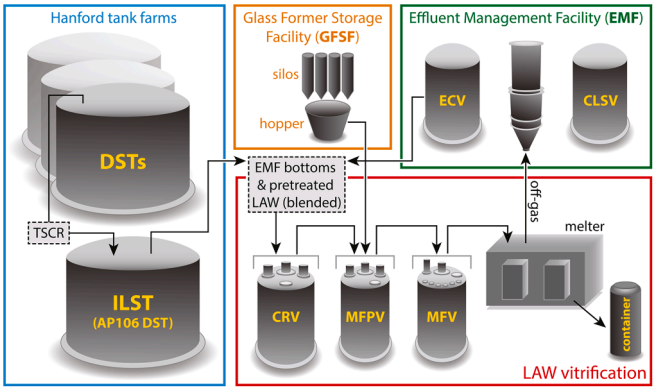

ARTICLE INFO

Keywords:
Nuclear Waste
Glass
Vitrification
Low-Level Waste
Hanford
Formulation
Melter
Process

ABSTRACT

This paper summarizes the vast body of literature (over 200 documents) related to vitrification of the low-activity waste (LAW) fraction of the Hanford tank wastes. Details are provided on the origins of the Hanford tank wastes that resulted from nuclear operations conducted between 1944 and 1989 to support nuclear weapons production. Waste treatment processes are described, including the baseline process to separate the tank waste into LAW and high-level waste fractions, and the LAW vitrification facility being started at Hanford. Significant focus is placed on the glass composition development and the property-composition relationships for Hanford LAW glasses. Glass disposal plans and criteria for minimizing long-term environmental impacts are discussed along with research perspectives.

1. Introduction

The U.S. Department of Energy (DOE) Office of River Protection (ORP) currently manages over 210,000 m^3 of highly radioactive wastes in underground tanks at the Hanford Site in southeast Washington state [1,2]. The waste was generated as a byproduct of reprocessing nuclear fuels and targets from 1944 through 1989 [3,4]. As a result of various processes used during that period, the resulting waste is complex and varies widely. To handle such a complex problem and prevent release of this waste into the surrounding environment, vitrification was selected

* Corresponding author.
E-mail address: john.vienna@pnnl.gov (J.D. Vienna).

https://doi.org/10.1016/j.jhazmat.2023.132437
Received 8 June 2023; Received in revised form 8 August 2023; Accepted 28 August 2023
Available online 2 September 2023

to immobilize the waste, whereby the waste is converted into glass after being mixed with glass-forming chemicals (GFCs). Glass can be produced on a commercial scale with well-vetted melter technology [5–8], is known for tailorable properties [9–14], and can be designed with chemical durability sufficient to immobilize radionuclides for millions of years [15–19]. Glass has been extensively studied for decades, particularly for waste immobilization in the U.S. and in other countries [9,10,14,20–22]. Some of the data and information on the tank waste, waste treatment processes, and glass formulation history are in difficult-to-find sources such as government reports. Thus, the purpose of this article is to concisely summarize the critical points of the vitrification processes for the low-activity fraction of the Hanford tank waste and point interested readers to the wealth of additional data found primarily in government reports. Over 200 papers and reports were selected by a combination of reviewing open literature and government reports that speak to various aspects of Hanford LAW vitrification and following the documents cited in those reports and documents. A library search with key words of Hanford + low-activity waste + glass or vitrification or melter or formulation or process was performed few additional articles were obtained by this later search. The analysis of these documents was organized into logical topical areas as shown in the table of contents. Table S1 (Supporting Information) provides a lists the acronyms and abbreviations used within this review and their corresponding definitions.

2. Origins of Hanford site tank wastes

Hanford processed 96,900 tonnes of uranium (tU) fuels from 1944 through 1989, producing roughly 67 t of plutonium [3,4]. Originally, aluminum-clad uranium fuel was irradiated in one of eight (i.e., B, D, F, H, DR, C, KW, and KE) graphite-moderated, water-cooled reactors.[*] Additionally, from 1963 to 1987, the N Reactor irradiated zirconium-cladded fuel for both heavy metal production and electric power generation. The bismuth phosphate precipitation (BPP) process separated Pu from 8100 tU of fuel in T Plant and B Plant from 1944 through 1956. The reduction-oxidation (REDOX) solvent extraction process separated both Pu and U from 22,400 tU of fuel in S Plant from 1952 to 1967. The plutonium uranium reduction extraction (PUREX) solvent extraction process separated both Pu and U from 66,400 tU of fuel in A Plant from 1956 through 1972 and 1983 through 1989. During the progression from BPP → REDOX → PUREX, the tons of fuel processed per day increased extensively while the waste production decreased extensively as more efficient processing methods were developed. The dates when the Hanford reactors operated and the facilities where fuel was processed, as well as other processes, are summarized in more detail in Fig. S1 (Supporting Information). This is shown graphically in Fig. S2, and the distribution of waste (and types of wastes) produced by each process is shown in Fig. S3 and Table S2 of the Supporting Information. Photographs of these facilities along with key processing facilities are provided in Fig. S4–Fig. S14 of the Supporting Information.

Secondary processes also discharged waste to the Hanford tanks. Plutonium finishing was performed in Z Plant from 1945 through 1994. Uranium was separated from BPP byproducts in U Plant from 1952 to 1958 for reuse. The UO_3 Plant converted uranyl nitrate hexahydrate (UNH) to UO_3 for off-site shipping from 1952 through 1994. Strontium scavenging from tank waste took place in Hot-Semi-Works from 1961 to 1967 and in B Plant from 1968 to 1986. Cesium was recovered from tank waste and PUREX raffinate in B Plant from 1968 through 1986. The Al and Zr claddings were removed from the irradiated fuels in the head end of each of the main separation processes. More detailed histories of Hanford processes and their associated facilities can be found elsewhere [3,4,23,24–28]; the details are summarized in Fig. 1 and Fig. S1 (Supporting Information).

The wastes from all the Hanford processes described above were discharged to the tanks. As the tanks are constructed of carbon steel, they were first neutralized primarily using NaOH, then $NaNO_2$ was added for corrosion control. The neutralization caused precipitation of many components that are soluble in HNO_3 solution generating a slurry waste that was discharged to the tanks. Many of the tank farms operated with cascades, where neutralized wastes were directly discharged to the first tank with the overflow going to the second tank and so on. A total of ~2,000,000 m^3 of radioactive waste was discharged to the tanks between 1944 and 1990 [23]. In this timeframe, 190,000 m^3 was reprocessed, 455,000 m^3 was discharged to the ground after radionuclide removal, ~3800 m^3 leaked to the ground, and 1,100,000 m^3 was evaporated, leaving ~210,000 m^3 remaining in the tanks. Overall, the Hanford tank waste is primarily composed of sodium salts and, to a lesser extent, metal oxide and hydroxide sludge. Table 1 lists the primary waste constituents in the tanks according to the Best Basis Inventory [29].

The tank waste consists of three primary phases: supernatant, saltcake, and sludge; Fig. 2 shows examples of these. Supernatant is primarily sodium salts in solution, which reside in the double-shell tanks and in interstitial liquids in the single-shell tanks (SSTs) (Fig. 2a). This liquid is typically yellow and contains 50–90% H_2O with 10 M Na^+, 3 M NO_3^-, 2 M NO_2^-, 1 M OH^-, and 0.5 M $Al(OH)_4^-$ (with wide variations). The bulk water was removed from all the SSTs to reduce the risk of tank waste leaking. The dissolved salts in the SSTs precipitated to form a saltcake that is redissolved upon wet retrieval (Fig. 2b). Saltcake ranges in color from white to black, but is usually light brown, and contains 10–50% H_2O with precipitated salts (primarily $NaNO_3$, $NaNO_2$, $NaAl(OH)_4$). The Cs isotopes are primarily contained in the supernatant and saltcake phases. The insoluble metals precipitated from the tank waste, primarily in the form of oxides and hydroxides, form sludges (Fig. 2c). These sludges, which range from white to black but are usually reddish brown, contain roughly 50% H_2O and most of the metals (e.g., Al, Fe, Bi, Mn, Zr, Si, Sr, U, and transuranic elements). Some elements such as F, P, and Cr are split between sludge, saltcake, and supernatant.

3. Summary of the Waste Treatment Process

DOE-ORP has instituted the River Protection Project (RPP) to store, retrieve, treat, and dispose of the tank waste at the Hanford Site in a safe, efficient manner [1]. The cornerstone of the RPP is the Waste Treatment and Immobilization Plant (WTP), which is being designed, constructed, and commissioned by Bechtel National, Inc. under contract to ORP [30]. This plant has four major facilities: the Pretreatment Facility (PTF), the Low-Activity Waste (LAW) Vitrification Facility, the High-Level Waste (HLW) Vitrification Facility, and the Analytical Laboratory (LAB). The PTF will receive the tank waste and separate it into a LAW fraction with most of the waste mass (>90%) and an HLW fraction with most of the waste radioactivity (>95%). These separations include leaching of non-radioactive solid components, filtration of the remaining solids, and ion exchange of Cs from the liquid. The radioactivity of the LAW and supplemental LAW (described later in this section) combined is 4 MCi (148 PBq) from 132 MGal (499,674 m^3) or 296 GBq/m^3 while the radioactivity from the HLW is 101 MCi (3737 PBq) from 16 MGal (60,566 m^3) or 61,700 GBq/m^3 [1]. The LAW facility will receive the LAW fraction, mix it with GFCs to form melter feed, melt the feed to form an immobilized LAW glass, and treat the process gases. The HLW facility will receive the HLW fraction, mix it with GFCs to form melter feed, melt the feed to form an immobilized HLW glass, and treat the process gases. The LAB will analyze roughly 10,000 samples generated by WTP operations every year, supply data for safe and efficient operations, and qualify the glasses for disposal.

In addition to the four major facilities, several additional facilities support operations and maintenance of the WTP that, when combined, are referred to as the balance of facilities (BOF). To avoid starting all

[1] The naming convention for reactors and processing plants was selected for security, safety, and functional reasons.

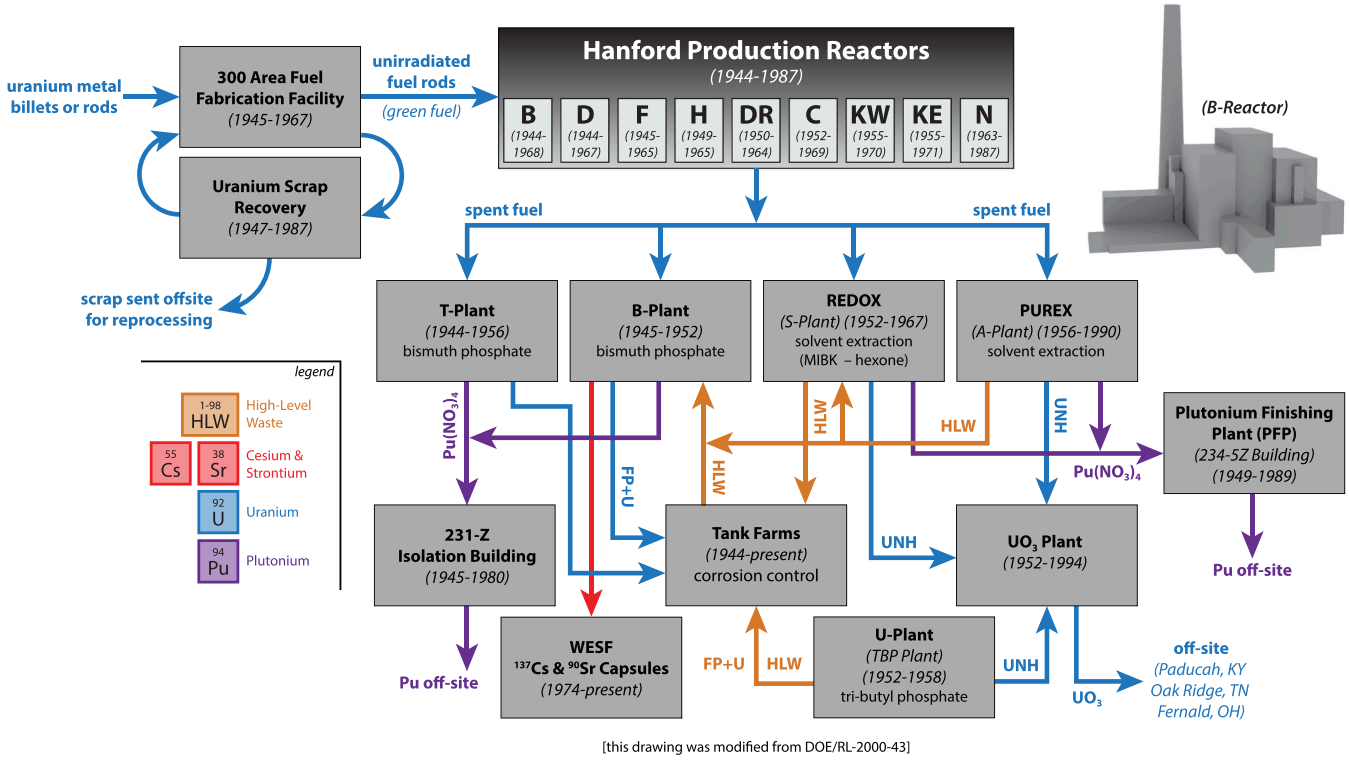

Fig. 1. Summary of processes contributing to Hanford tank waste. The values listed in parenthesis refer to the years of operation. Photographs of several of these facilities are provided Fig. S4– Fig. S14 of the Supporting Information. FP denotes fission products and MIBK denotes methyl isobutyl ketone.

Table 1
Tank waste chemical constituents from Best Basis Inventory [29] (excluding water and hydroxide). TOC denotes total organic carbon.

Ion	Mass%	Primary process contributing
NO_3^-	35.2	Nitric acid additions from fuel dissolution, BPP, REDOX, and PUREX
Na^+	31.8	Neutralizing, corrosion control, and solvent wash
NO_2^-	8.2	Corrosion control
CO_3^{2-}	6.7	Atmospheric absorption and solvent wash
Al^{3+}	5.6	Cladding removal and REDOX
PO_4^{3-}	3.2	BPP, THOREX, Cs/Sr recovery
SO_4^{2-}	2.3	BPP, REDOX, PUREX, Cs/Sr recovery
$C_2O_4^{2-}$	1.0	Oxalate precipitation
TOC	0.8	Several
F^-	0.8	Cladding removal, BPP, REDOX
Fe^{3+}	0.8	PUREX, BPP, REDOX, corrosion product
K^+	0.7	U recovery, solvent wash, neutralization, corrosion control
Cl^-	0.6	Chemical impurity, U recovery
Si^{4+}	0.5	Diatomaceous earth, PUREX, REDOX
U^{4+}, U^{6+}	0.4	BPP
Cr^{3+}, Cr^{6+}	0.4	BPP, corrosion control, corrosion products
Bi^{3+}	0.4	BPP
Zr^{4+}	0.3	Cladding removal
Ca^{2+}	0.2	Several
Other	0.1	Includes nearly the entire periodic table

four major facilities at the same time, DOE implemented a staged startup approach [31]. The phased approach allows DOE to balance staffing demands and apply resources to address technical issues likely to occur during startup and commissioning of each facility. This approach leads to the startup of the LAW facility first under a direct-feed low-activity waste (DFLAW) configuration. To successfully operate the LAW facility under DFLAW, two other facilities were added: the Tank-Side Cesium Removal (TSCR) Facility and the Effluent Management Facility (EMF). TSCR removes radioactive Cs isotopes using an ion exchange process and radioactive Sr and transuranic containing solids using filtration. The EMF is designed to evaporate LAW facility liquid effluents into concentrated and dilute streams for recycle and treatment/disposal, respectively, using evaporation.

To complete the full RPP mission efficiently, there may be need for a supplemental low-activity waste treatment capability (SLAW) [1]. The SLAW facility will treat the LAW fraction that is generated at a rate above which the LAW facility can process. The baseline SLAW facility will be a second LAW vitrification facility. However, alternative treatment technologies, such as grout, bulk vitrification, and fluidized bed steam reforming, have been proposed as alternatives [32–34].

At the time of writing this paper, these facilities (summarized in Table 2) are each in a different state of design, construction, component testing, commissioning, and operations. Notably, design and construction are complete for those facilities required for DFLAW (LAW, TSCR,

Fig. 2. Photographs of (a) supernatant in a laboratory sample, (b) saltcake, and (c) sludge taken inside of a tank.

Table 2
Summary of the primary facilities existing (or planned) at the WTP.

Facility name	Abbr.	Description
Pretreatment Facility	PTF	Receives waste and separates it into LAW and HLW
Low-Activity Waste Vitrification Facility	LAW	Receives LAW, mixes with GFCs, vitrifies mixture to form immobilized low-activity waste (ILAW) glass, treats process gases
High-Level Waste Vitrification Facility	HLW	Receives HLW, mixes with GFCs, vitrifies mixture to form HLW glass, treats process gases
Analytical Laboratory	LAB	Analyzes samples from WTP operations, supplies data for safe operations, qualifies glass for disposal
Tank-Side Cesium Removal Facility (operated by Tank Farm Contractor)	TSCR	Removes radioactive Cs, Sr, and transuranics and delivers decontaminated LAW to LAW facility
Effluent Management Facility	EMF	Evaporates LAW liquid effluents into concentrated and dilute streams for recycle and treatment/disposal, respectively
Supplemental LAW Treatment (to be designed and built)	SLAW	Operation to treat LAW fractions over the treatable fraction

EMF, LAB, and portions of BOF). TSCR is currently operating [35], and the LAW facility, EMF, LAB, and BOF are in the testing phase, with commissioning planned to begin in 2023. Fig. 3 shows a schematic of the DFLAW process and Fig. 4 shows an aerial photograph of the WTP.

The pretreated LAW fraction of the waste contains the sodium salts after solids (including Sr and transuranic elements) and Cs removal. The composition of LAW varies from batch-to-batch as shown in Fig. 5. Of particular interest to the LAW batch compositions are the relatively large composition differences and abrupt changes between batches that need to be managed by the LAW vitrification process.

DFLAW vitrification is divided into several processes. The LAW concentrate receipt process (LCP) will receive the LAW from the interim LAW storage tank (ILST, tank 241-AP-106; see Fig. 3a) and the DFLAW EMF process (DEP) into each of two concentrate receipt vessels (CRVs). Each CRV can hold between 48.661 m^3 (12,855 gal) and 56.312 m^3 (14,876 gal) of LAW with a nominal batch size of 34.50 m^3 (9115 gal). After receipt of waste, the CRV is mixed with a 40-horsepower agitator and sampled. Chemical analysis of the waste is used to determine the target glass composition to be produced. LAW is then transferred to the melter feed preparation vessels (MFPVs).

The LAB will receive, manage, and analyze 952 LAW and 81 BOF samples per year during DFLAW. During full coupled operations over 10,000 samples will be analyzed in the laboratory [37]. The composition of the LAW/EMF bottoms in each CRV batch will be analyzed using inductively-coupled plasma optical emission spectroscopy and mass spectroscopy, α counting, β counting, γ energy analysis, ion chromatography, liquid scintillation counting, and persulfate oxidation [37].

The immobilized LAW (ILAW) glass composition is formulated based on the analyzed composition of LAW samples taken from the CRV. Glasses are formulated to simultaneously satisfy several processing and product quality-related constraints by methods described in Section 5. The outcome of glass formulation is a recipe with the volume of waste to transfer from the CRV to the MFPV and the mass of each GFC to add to the MFPV batch (see Fig. 3).

The LAW melter feed process (LFP) will receive LAW from the CRV into one of two MFPVs. Each MFPV can hold between 19.43 m^3 (5132 gal) and 28.35 m^3 (7489 gal) of melter feed with a nominal batch size of 12.87 m^3 (3400 gal). After receipt of the LAW, GFCs from the glass former reagent process (GFR) are mixed into the LAW plus melter feed heel. A sample of melter feed is taken for use in process control and the melter feed is transferred into the melter feed vessel (MFV) as a batch. The melter feed is fed into the melter (within the LAW melter process, LMP) through six water-cooled feed nozzles. Each nozzle is fed by an independent air-displacement slurry pump within the MFV.

The GFR receives, weighs, blends, and transfers batches of GFCs. There are currently 12 silos (see Fig. 3a,c) planned to feed GFCs to the LFP that include silica (SiO_2), boric acid (H_3BO_3), zincite (ZnO), rutile (TiO_2), zircon ($ZrSiO_4$), kyanite (Al_2SiO_5), wollastonite ($CaSiO_3$), olivine (Mg_2SiO_4), hematite (Fe_2O_3), lithium carbonate (Li_2CO_3), sodium carbonate (Na_2CO_3), and sucrose ($C_{12}H_{22}O_{11}$). Each GFC is weighed and transported to the blend hopper, where a complete GFC batch is weighed, blended, and transported pneumatically to the LAW glass former mixer. The GFC batch is weighed and mixed with roughly 4 mass % water (for dust control) and transferred to the MFPVs.

The LMP includes two melters [38]. Each melter is self-contained and shielded with outer dimensions of 8.99 m (29.5 ft; length), 6.55 m (21.5 ft; width), and 4.80 m (15.75 ft; height) and weighs roughly 300 t (empty). The liquid-fed ceramic-lined melters (LFCMs) are lined with two layers of Monofrax™ K-3 refractory on most glass-contact surfaces (Monofrax™ E on some surfaces) that are 30.5 cm (12 in.) and 12.7 cm (5 in.) thick, respectively. Heat is conducted relatively easily through this dense corrosion-resistant refractory layer. A double layer of Zirmul® refractory reduces heat conduction (e.g., a thermal insulator). The refractories are electrically isolated from a water-cooled shell using a thin insulating layer. The melt pool dimensions are 4.93 m × 2.03 m (16 ft 2 in. × 6 ft 8 in.), and the melt height is nominally 0.762 m (2 ft 6 in.) but varies with feeding and pouring cycles (containing roughly 7000 L of melt or roughly 15 t). The headspace is lined with Monofrax™ H refractory. There are three sets of apposing Inconel 690 electrodes that power the melter to maintain a target 1150 °C melt temperature. Melter feed is introduced through six feed nozzles and the slurry melter feed dries to form a cold-cap across most of the 10 m^2 melt surface. Heat from the roughly 0.76 m (2.5 ft) deep melt is transferred to the cold-cap bottom and converts the dried feed into a silicate-based liquid. The

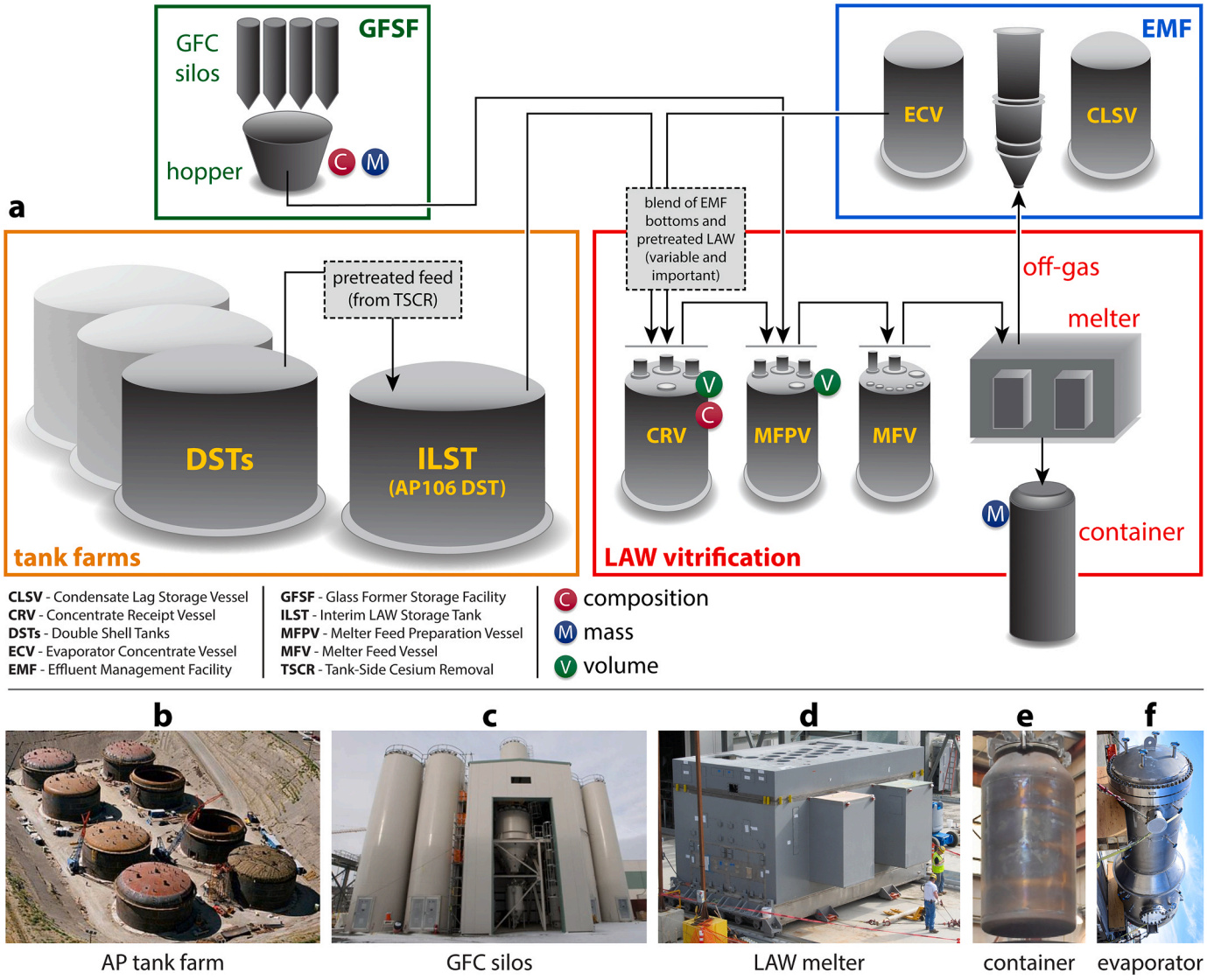

Fig. 3. (a) Simplified flowsheet of DFLAW at the WTP where one of two LAW treatment trains is shown within the LAW facility. (b-f) Pictures of various parts of the facility including (b) the AP tank farm, (c) the glass-forming chemical (GFC) silos, (d) the LAW melter, (e) the LAW container, and (f) the evaporator. The C, M, and V indicate composition, mass, and volume measurements, respectively, performed as part of the waste form control and acceptance process.

melt is agitated by bubbling of air through 18 bubblers introduced from above the glass melt. The glass melt is cast by airlift through one of two pour spouts into 304 L stainless-steel containers, where it cools and solidifies to form an ILAW glass. Each melter discharges roughly 15 t of glass per day, filling almost three containers (see Fig. 3a,e) with 6 t of glass each. Meanwhile, process gases exit the top of the melters into the LAW off-gas process.

Container handling includes container receipt, filling, level detection, inert fill, cooling, transfer, sampling (if required), lidding, contamination survey, decontamination (if required), transfer, weighing, and exporting. The 2.29 m (7.5 ft) tall and 1.22 m (4 ft) diameter stainless steel containers are filled to over 90 vol% level with nominally 6 t of glass. If the glass fill level is insufficient, an optional inert material (SiO_2) backfill is added to bring the total fill volume to $\geq$90 vol%.

Gases exit the top of each melter through a film cooler, which injects air to cool the gas from a melter headspace temperature of between 400 and 500 °C to roughly 315 °C. The gas travels through a transfer line into a submerged bed scrubber (SBS) that cools the gas from roughly 280 °C to about 100 °C and condenses off-gas components. The gases exiting the SBS are fed into a wet electrostatic precipitator (WESP). Within the WESP, power is applied across electrodes, gases are ionized, and ions are accelerated to plate collectors to remove sub-micrometer particles [39,40]. The condensed gas components in the SBS are combined with the WESP particulate matter deluge into a collection vessel that will be processed in the EMF. Gases exiting the WESPs on each melter train will be combined with vessel vent off-gases and then treated in the LAW secondary off-gas and vessel vent process (LVP). The combined LVP gases are heated and passed through a bank of high-efficiency particulate air (HEPA) filters. Mercury is then removed in a granulated activated carbon bed. A thermal catalytic oxidizer removes organics, and a selective catalytic reducer converts NO_x to N_2 using NH_3. Residual acid gases are then removed in a caustic scrubber and gas is discharged through a stack using exhaust blowers.

The liquid condensate is transferred to the EMF, where it is concentrated in an evaporator. The evaporator bottoms are recycled back to the LAW facility, while the overheads are condensed and blended with the caustic scrubber solution for discharge to the Liquid Effluent Retention Facility and Effluent Treatment Facility for further treatment and discharge.

Fig. 4. Aerial photograph of WTP facing west taken in 2020 (snowcaps of Mt. Rainier and Mt. Adams in the distance).

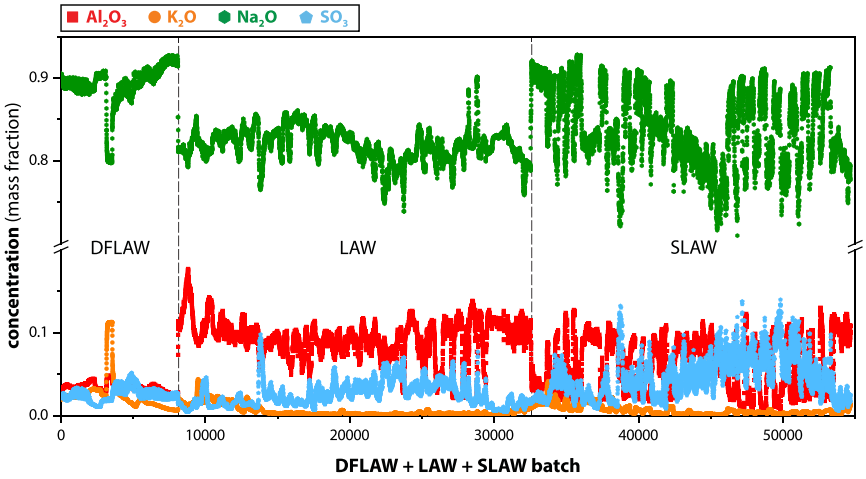

Fig. 5. Major waste component concentrations as functions of batch number, where the first ~8790 batches of LAW are from the DFLAW phase and the latter are for SLAW. This figure was modified from Lu et al. [36] and reprinted with permission. Copyright Elsevier 2021.

4. LAW vitrification melter technology history

The melters designed for use in the WTP LAW facility will be the largest LFCMs for glass production deployed anywhere in the world. The melters were developed considering current glass melting capabilities used in the glass manufacturing industry as well as the magnitude of the immobilization effort required at the WTP to vitrify 210,000 m^3 of waste. Previous LFCMs were used in West Valley Demonstration Project (WVDP, in New York), Savanah River Site (SRS, in South Carolina) M Area, and for ongoing vitrification efforts at the Defense Waste Processing Facility (DWPF, in South Carolina) [41–45]. Lessons learned from operation and, in the case of WVDP and SRS M Area, decommissioning were applied in the design of the WTP LAW melters [38].

The melter design life is 5 years. However, based on performance of DWPF and WVDP, it is anticipated that lifetimes of 7–10 years are likely. Bubbler changes are anticipated every 6 months. The constraints that

Table 3
Summary of glass property constraints, the associated limits, and the driver for why the limit exists.

Property	Limit	Driver	Ref.
Melt viscosity at 1150 °C (η_{1150})	$2 \leq \eta_{1150} \leq 8$ Pa•s	Process efficiency, mixing, and corrosion	[46]
Melt viscosity at 1100 °C (η_{1100})	$\eta_{1100} \leq 15$ Pa•s	Pouring and idle process efficiency	[47]
Melt electrical conductivity at 1100 °C (ε_{1100})	$\varepsilon_{1100} \geq 10$ S•m^{-1}	Power delivery to the melt	[47]
Melt electrical conductivity at 1200 °C (ε_{1200})	$\varepsilon_{1200} \leq 70$ S•m^{-1}	Current density on electrodes	[47]
Melt crystal content at 950 °C (C_{950})	$C_{950} \leq 1$ vol%	Melter pour spout pluggage	[47]
6-d Monofrax K3 refractory corrosion (k_{1208})	$k_{1208} \leq 0.00102$ m	Melter lifetime	[48]
Sulfur solubility/sulfur concentration (S/C)	S/C ≥ 1	Excessive corrosion of melter components	[49]
Product consistency test (PCT) response normalized Na, B, and Si losses ($NL_{[Na,B,Si]}$)	$NL_{[Na,B,Si]} \leq 2$ g•m^{-2}	Reduce risk of excessive corrosion rate in the Integrated Disposal Facility (IDF), Specification 2.2.2.17	[30]
Vapor hydration test (VHT) alteration rate (r_a)	$r_a \leq 50$ g•m^{-2}•d^{-1}	Reduce risk of accelerated corrosion in the IDF, Specification 2.2.2.17	[30]
Phase changes during slow cooling in the container	No significant impact to performance	Ability to satisfy disposal criteria	[50]
Waste classification (W_C)	$W_C \leq$ class C	Demonstrate waste is incidental to reprocessing, Specification 2.2.2.8	[50]
^{90}Sr activity	^{90}Sr ≤ 20 Ci•m^{-3}	Demonstrate waste incidental to reprocessing (WIR), Specification 2.2.2.8	[50]
^{137}Cs activity[(a)]	^{137}Cs ≤ 3 Ci•m^{-3}	Demonstrate WIR, Specification 2.2.2.8	[50]
^{137}Cs activity[(a)]	^{137}Cs ≤ 0.3 Ci•m^{-3}	Contact maintenance dose, Section C.7	[50]
Container surface dose rate (D_S)	$D_S \leq 500$ mrem•h^{-1}	Container handling, Specification 2.2.2.9	[50]
Land disposal restrictions (LDR)	Satisfy petition	IDF acceptance criteria, Specification 2.2.2.20	[50]

(a) There are two ^{137}Cs constraints in the contract. One is required for waste disposal while the other for contact maintenance. The higher limit determines the maximum that can be put in glass while the lower can potentially be exceeded on a case-by-case basis if process safety can otherwise be assured.

have been enacted as requirements include K-3 corrosion rate, viscosity (η), electrical conductivity (ε), and sulfur solubility (see Table 3). These constraints are further discussed in Section 6.

Prior to the down-selection of the LFCM technology in 1999, there was an effort to reach out to various commercial melter vendors to test different melter technologies that included Joule-heated ceramic melters (GTS Duratek, Envitco, Pemberthy Electromelt, and Vectra Technologies), gas-fired cyclone burner furnaces (Babcock & Wilcox), plasma torch cupola furnaces (Westinghouse), and electric arc furnaces (U.S. Bureau of Mines) [51]. At the time that the companies were engaged, there was also an effort to determine what the reference glass (es) should be so that compositions could be tested in the melters [52,53]. If companies were going to melt their own glasses, then the glass performance needed to be confirmed. Additionally, initial formulated glasses had higher melting temperatures (~1300 °C) as they were high in Al_2O_3 and SiO_2 and lower in B_2O_3. Also, a shift was made to investigate soda-lime silicate glasses and large, gas-fired melters. At this time, it was thought that off-gas systems may be simplified due to low radioactivity, although the possibility of scrubbing was considered. Later, it would be realized that off-gas systems will be critical in treating chemical hazards (such as NO_x) and trapping semi-volatile radionuclides for recycle.

After selection of the JHCM for Hanford LAW vitrification, evaluation was performed for the next generation LAW melter [54]. The alternative technologies considered included the Cold Crucible Induction Melter and an advanced JHCM. The advanced JHCM proceeded to design. Later evaluations were also performed to consider supplemental LAW (SLAW) treatment technologies, that is to treat the fraction of Hanford LAW that exceeds the capacity of the LAW vitrification facility [32,33]. Potential SLAW treatment technologies considered include: 1) a second LAW vitrification facility like the first one based on next generation JHCMs [55], 2) a fluidized bed steam reformer similar to the Idaho Waste Treatment Unit only producing a granular aluminosilicate waste form [56,57], 3) a GeoMelt™-based bulk vitrification system [58–60], and 4) a cementitious grout system [61]. To date, no decision has been made as to which of these technologies to deploy [34].

5. Glass formulation in support of WTP

Glass compositions are formulated to simultaneously satisfy several property and composition constraints selected to efficiently process the waste and protect the environment in the selected disposal facility. Table 3 summarizes the current LAW glass/melt property constraints. Section 6 and Section 7 describe these constraints in more detail along with composition effects on their values.

The methodology for formulating glass compositions for Hanford LAW immobilization has progressed significantly over the life of the project. The first Hanford ILAW glass formulations were reported by Kim et al. [52] and Feng et al. [53] under the Tank Waste Remediation System (TWRS) project. These formulations assumed a reasonably constant LAW composition represented by an analyzed dissolved saltcake sample. The glass property constraints assumed a high-temperature ($T_M \geq 1300$ °C) melter with durability constraints comparable to the then-current U.S. HLW glass standards of Materials Characterization Center test 1 (MCC-1) and product consistency test (PCT). Upon privatization of the Tank Waste Remediation System (TWRS-P), individual glass compositions were designed to immobilize each of three waste compositions (envelopes A, B, and C) using an Edisonian trial-and-error approach [62]. The compositions of the envelopes are primarily divided by the mass ratios of SO_3 to Na_2O in waste: A) SO_3:$Na_2O < 0.035$, B) SO_3:$Na_2O > 0.070$, and C) $0.035 \leq SO_3$:$Na_2O \leq 0.070$. Additionally, envelope C contains soluble Sr and transuranics that would be removed in the PTF. The durability requirements during TWRS-P included a 20 °C, 7-day PCT response and the leachability index (ANSI-16.1) [63]. In 2000, a performance assessment concluded that it was possible for ILAW glasses to satisfy the TWRS-P contract durability requirements (20 °C PCT and ANSI-16.1) yet fail to meet disposal performance goals. The durability constraints were changed to 90 °C PCT and vapor hydration test (VHT) responses of 2 g•m^{-2} and 50 g•m^{-2}•d^{-1}, respectively [30]. Additionally, it became apparent that the anticipated range of waste compositions was not likely to be successfully immobilized with only three glass compositions, so envelopes A, B, and C were divided into eight sub-envelopes based on the ratios of SO_3:Na_2O and K_2O:Na_2O and glasses were formulated for each [64]. Plant process model results showed that the waste composition was likely to be significantly more variable than previously planned, and a continuum approach to glass formulation was developed [65] and later improved [66]. This continuum glass formulation correlation interpolates between the eight sub-envelope glass compositions that have been successfully demonstrated up to 1/3 pilot-scale [67].

Fig. 6 shows a schematic of the composition correlation. The loading is determined by the mass ratio of NaK = $Na_2O + 0.66\ K_2O$ to SO_3 in the waste. A line can be drawn from the origin of Fig. 6a with the slope equal to the waste ratio NaK:SO_3, and the point where it strikes the red line will determine the NaK and SO_3 content in the target glass composition. For example, a waste represented by the dashed blue line in Fig. 6a would target 18.85 mass% NaK and 0.4 mass% SO_3. Note that the allowable SO_3 concentration may be reduced by higher concentrations

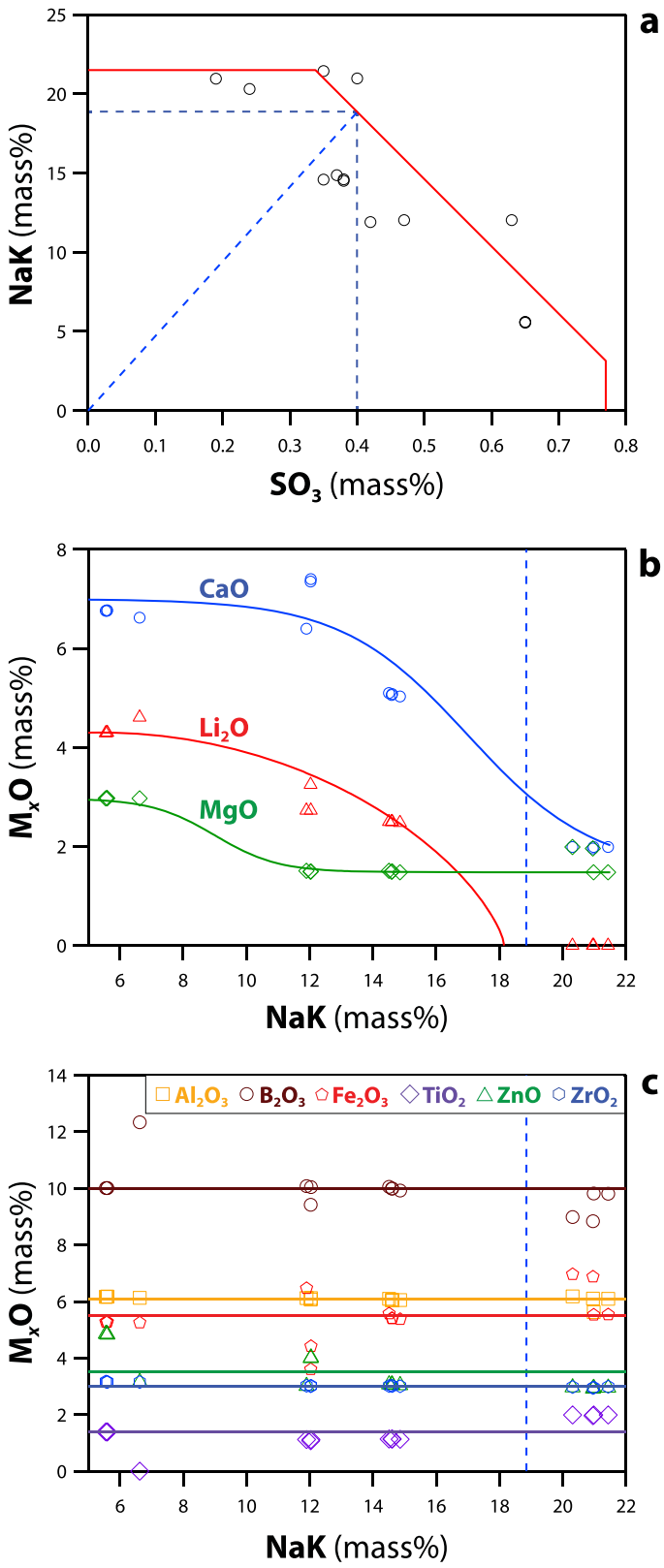

Fig. 6. WTP baseline glass formulation correlation (after Kim and Vienna [50]) including (a) NaK vs. SO_3, (b) M_xO vs. NaK, and (c) M_xO vs. NaK where M_xO denotes (metal oxide) and NaK = Na_2O + 0.66 K_2O (mass basis). The lines in (a) describe a boundary of NaK and SO_3 (red line) and the blue dotted lines represent the NaK and SO_3 content in an illustrative example glass. The lines in (b) and (c) represent the target concentrations of each associated oxide in glass.

of Cl, P, and Cr_2O_3. Other waste components are added to glass in proportion to their concentrations in waste. Using the target NaK concentration, the concentrations of MgO, Li_2O, and CaO can be calculated using the functions shown in Fig. 6b. The concentrations of Al_2O_3 (6.1 mass%), B_2O_3 (10.0 mass%), Fe_2O_3 (5.5 mass%), TiO_2 (1.4 mass%), ZrO_2 (3.0 mass%), and ZnO (3.5 mass%) are held constant at the levels shown in Fig. 6c. Finally, the concentration of SiO_2 is determined as 100 minus the sum of mass% of all other components. Kim and Vienna [50] describe the details of how these formulations are to be implemented in plant operation. This is a significant advancement in the state-of-the-art as it allows, for the first time, real-time glass formulation during plant operation.

This baseline approach to glass formulation was developed specifically to commission the LAW facility and therefore does not optimize the loading of waste in glass. Increasing the loading of waste in glass will reduce the cost of treating the tank waste by reducing the total number of ILAW containers and, if needed, the capacity of an SLAW facility. To obtain a more reasonable estimate of glass mass and associated mission impact, a glass loading model of 20 mass% Na_2O and 0.8 mass% SO_3 was used for early system planning [68]. This limit is based on Idaho National Laboratory's sodium bearing waste glass formulations [69–71].

In 2016, Vienna et al. [72] expanded and updated the glass formulation approach and models for use in Hanford system planning. These models resulted in a significant increase in loading of LAW in glass with NaK and SO_3 concentrations of 24 and 1.5 mass%, respectively. The approach to ILAW glass formulation also changed to a numerical optimization approach where each of the constraints listed in Table 3 are expressed as functions of glass composition and a maximum waste loading is calculated using numerical optimization methods. Using this method, a glass processing envelope is mathematically defined with models and uncertainties (shown schematically in Figure S15, Supporting Information). The approach to implementing these models was described by Lumetta et al. [73] and used for the Hanford system planning from 2016 through 2020. Due to the maximum constraints on NaK and SO_3, unique solutions for glass composition could not be obtained for many of the waste compositions. Muller et al. [74] developed a correlation similar to the baseline formulation method to identify unique glass compositions for each waste at the higher waste loadings. In this correlation, three new GFCs were proposed, including V_2O_5 to improve sulfur solubility, SnO_2 to reduce r_a, and Cr_2O_3 to reduce the K-3 corrosion rate. The approach to implementing this method in plant operation is described by Lumetta et al. [73].

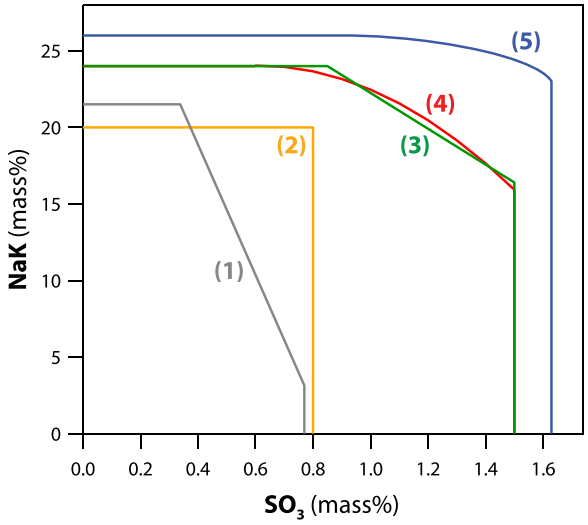

Fig. 7. Waste NaK (=Na_2O+ 0.66 K_2O) and SO_3 loading (mass%) including (1) the WTP baseline [66], (2) data from Hamel et al. [68], (3) data from Vienna et al. [72,77], (4) data from Muller et al. [74], and (5) data from Vienna et al. [75].

In 2022, Vienna et al. [75] developed a set of glass property models and constraints for plant operations where models were included for all the constraints listed in Table 3. The approach for implementing the models is the numerical optimization technique and, since the NaK and SO_3 data limits are significantly higher than those of the 2016 models (27 and 1.63 mass%, respectively), nearly all example wastes do generate unique optimal glass compositions. The implementation of the optimization is described by Lumetta et al. [76]. The glass compositions were calculated for wastes shown in Fig. 5. These compositions are shown in Figure S16 (Supporting Information) as functions of NaK and SO_3. Fig. 7 compares the loading of waste NaK and SO_3 between the different formulation methods.

The application of glass property-composition models and plant operating data to specify glass formulations and qualify ILAW glass for disposal is performed in algorithms and software routines [50,78–80]. These routines estimate both prediction and process uncertainties to define the processing envelope and optimize the glass (see Figure S15, Supporting Information). The uncertainty quantification (UQ) methods applied include confidence intervals for processing related property prediction uncertainties, simultaneous confidence intervals for product-quality-related property prediction uncertainties, and Monte-Carlo simulations for process and composition uncertainties. The combined uncertainties have been found to significantly restrict the processing envelope size and efforts are underway to reduce property prediction uncertainties.

6. Processing properties and constraints

6.1. Viscosity

The viscosity (η) of the glass-forming melt impacts the processability of the melter feed during conversion into glass within the melter [81] and impacts the final pouring of the glass melt out of the melter into the containers [82]. The viscosity of a liquid, in this context as a glass melt, describes the resistance to flow. If the melt viscosity is too low (i.e., $\eta < 2$ Pa•s) at the melter operating temperature of 1150 °C, melts tend to exhibit greater volatility, more corrosion of contact materials (e.g., refractories, electrodes, bubblers, thermowells, level probes), and faster settling of crystalline phases. If the viscosity of a glass melt is high (e.g., $\eta > 8$ Pa•s), then the glass production rate will decrease, partially due to the slower mass transfer within the melter and partially due to the greater tendency to trap evolved gases from melter feed reactions, resulting in foaming [82].

Higher melt viscosities introduce difficulties in pouring a glass melt, which also impact the filling of the containers. Glass viscosity is typically measured using a torque viscometer immersed in a glass melt at temperatures within 200 °C of the melting temperature [83]. Melt viscosities vary smoothly with temperature [82]. Over narrow viscosity ranges, the temperature effect can be approximated using a linear correlation between logarithm viscosity and inverse temperature (Arrhenius correlation) [82,84–88]. The data show significant curvature when considering broader viscosity ranges. The trends have been described using Vogel-Tammann-Fulcher (VFT) [82,89,90], Avramov-Milchev [82,91], Mauro-Yue-Ellison-Gupta-Allan (MYEGA) [82], and Gibbs-Adams [92,93] relationships.

Glass components such as Al and Si are known to increase melt viscosity while B, Fe, alkali, and alkaline earths are known to decrease the melt viscosity. The glass networks of ILAW glasses are mostly composed of Si–O bonds, the primary glass-forming moiety. In traditional glass science, Si is considered a *network-forming* cation based on its cationic field strength value, which is > 1.3 $Å^{-2}$ [94]. The cationic field strength is expressed as z/a^2, where z is the cationic valence and a is the interatomic distance to an O^{2-} anion [95]. Therefore, the cation field strength index is an arbitrary scale relative to other metrics such as the optical basicity (which describes the ability of the glass network to donate

charge) and the number of non-bridging oxygens per tetrahedra (which is a measure of network rigidity), but these metrics require more assumptions and are less accurate [95]. Alkali and alkaline earth cations, which disrupt the glass network, are considered *network modifiers* and have a field strength < 0.4 Å^{-2} [94]. Components such as Al and Fe are considered to be *network intermediates* that can either enter or disrupt the glass network, depending on the chemistry of the melt, and possess field strength values of 0.4–1.3 Å^{-2} [94]. For ILAW glasses, Fe and Al are primarily in the four-coordinated network-forming configuration. For most glass components, the classification as a network former, intermediate, or modifier correlates with the tendency to increase or decrease viscosity. One exception to this is B, which is classified as a network former but decreases the melt viscosity in ILAW glass melts. Quantitative estimates of composition and temperature effects on ILAW glass melt viscosity are reported in the literature [75,82,84–88,91,92].

An alternative method to estimate and predict glass melt viscosity employs aggregator functions (specifically the minimum value, maximum value, or standard deviation) to combine the effects of glass composition and 35 chemical features of the glass melt (including atomic radius, atomic volume, fusion enthalpy, etc.), which are fed into an artificial neural network (ANN) algorithm [96]. This ANN algorithm can then be utilized to output the viscosity model coefficients for various viscosity equations including the MYEGA [97] equation and the VFT equation [98–100].

6.2. Electrical conductivity

Electrical conductivity (ε) of the melt is critical as Joule-heating using Inconel 690 electrodes, is used to heat the melter [38,50,101]. During Joule-heating, electrical current is supplied to electrodes immersed within a glass melt. The electrical resistivity of the glass melt impedes the conduction of the electrical current, producing heat. The electrical conductivity must be maintained at $\varepsilon > 10$ S m^{-1} at 1100 °C and $\varepsilon < 70$ S m^{-1} at 1200 °C [50,75]. Values of $\varepsilon < 10$ S m^{-1} at 1100 °C limit the electrical power that can be delivered to the melt to maintain temperature and processing rate while values of $\varepsilon > 70$ S m^{-1} at 1200 °C could exceed the current density limits for the electrodes [75]. Formation of a segregated salt layer (primarily composed of molten sulfate salt and commonly referred to as *yellow phase* or *gall*) on top of the reacting melter feed can pose issues due to the relatively high electrical conductivity of sulfate salt ($\varepsilon \approx 6900$–1500 S m^{-1} at 800 °C) [102]. The high electrical conductivity of the segregated salt layer may increase the risk of power disruptions, as discussed in Section 6.3. Electrical conductivity is typically measured between two platinum plates immersed in molten glass at temperatures near melting temperature [103].

Electrical conductivity varies smoothly with temperature. Over narrow conductivity ranges, the temperature effect can be approximated using an Arrhenius correlation [77,90,104]. The data show some curvature when considering broader conductivity ranges. However, as conductivity is only pertinent to Joule-heating at melt temperature range, non-linearities are not significant for this application. At a given temperature, the components Li and Na are known to increase the electrical conductivity because these cations serve as charge carriers. These cations are coulombically bonded to non-bridging oxygens in the glass melt and have a high relative mobility [94]. Of the elements present in ILAW glass melts, Si is known to have the largest negative impact on the electrical conductivity, likely due to the dilution of charge carriers [75].

6.3. Sulfur solubility

Sulfur solubility is another parameter affected by the glass composition, which in turn affects the lifetime of melter components. If the sulfur solubility is below the melter feed concentration, a sulfate-enriched salt layer could form, which can corrode melter components such as the bubbler, electrodes, and the K-3 refractory [49,75,105,106]. Additionally, as described in Section 6.2, the high electrical conductivity of the molten salt phase can result in electrical short-circuiting [102]. Melter SO_3 tolerance (a measure of the maximum fraction of SO_3 that can be introduced into a melter without the formation of a segregated sulfate phase) has been experimentally determined through a variety of crucible methods, including batch saturation, saturation re-melting, bubbling a melt with an SO_2-O_2 gas mixture (also known as the *gas saturation* method), melter tolerance, and three-time saturation [75]. These crucible methods provide an inexpensive way to determine SO_3 tolerance within the large-scale melter [75,107]. The constraint for sulfur solubility/concentration (S/C) ratio is ≥ 1 (see Table 3).

Components such as Li, Na, Ca, and V have been observed to increase the sulfur solubility while Cl and Cr decrease the sulfur solubility [75]. The cation field strength index, which is a summation of the field strengths of all cations in a glass, has a strong correlation to the ability of the glass network to accommodate SO_4^{2-} into the glass network [94,95]. However, the cationic field strength index also correlates with the fraction of alkali cations, which are needed in order to charge-compensate SO_4^{2-} when it is incorporated in the glass melt [95]. The addition of vanadium to glass has been observed to enhance the solubility of sulfur, despite not following the cation field strength trend and there being no evidence that V–S or V–SO_4^{2-} bonds are present in V_2O_5-containing ILAW glasses [49,82,95,108–110]. Two theories attempt to describe this effect. The first theory, proposed by Stefanovskii et al. [111,112], uses the following inputs: the cationic field strengths, the cation-oxygen binding energy, the bond strength (z/k where z is charge and k is coordination number), as well as the size and polarization of the cation polyhedra. With these inputs, the cations in a hypothetical glass structure follow the series $^{[4]}S^{6+} > {}^{[5]}P^{5+} > {}^{[4]}V^{5+} > {}^{[3]}B^{3+} > {}^{[4]}Si^{4+} > {}^{[4]}B^{3+} > {}^{[4]}Al^{3+}$, where the number in brackets is the coordination number and the number on the right is cationic charge. Within this series, cations that are closer exhibit greater chemical compatibility; hence, vanadium-rich glasses were believed to better incorporate sulfate tetrahedra than glasses composed of silicate tetrahedra. The second theory, proposed by Manara et al. [95,109,113], suggests that within sulfate-bearing borosilicate glasses, vanadium depolymerizes the borate network and promotes the formation of voids whose shape and size are compatible with the sulfate polyhedral units.

In addition to composition effects, sulfate solubility is impacted by temperature and REDOX state of the melt. As a function of increasing temperature, sulfate can decompose from the interface of sulfate salts and the atmosphere or from the interface of the glass melt and the atmosphere [114]. Temperature also affects the activity of free oxygen and the sulfur solubility within the glass melt. These factors are a function of glass composition and the oxidation state of the glass melt. The REDOX state of the melt can be controlled using reducing agents such as sucrose. The more reducing the melt, the higher the fraction of sulfate that is converted to sulfite, which partitions to the melter off-gas [70,115–119].

For routine ILAW glass production, the target SO_3 fraction within the melter feed is greater than the final measured fraction due to the evolution of SO_2 gas during glass melting [75]. The SO_3 fraction in the final glass can either be measured using a variety of characterization tools (e.g., inductively coupled plasma-optical emission spectroscopy [ICP-OES], X-ray fluorescence, or electron probe microanalysis) or estimated using an empirical SO_3 measured-target equation [75]. WTP baseline glasses are designed specifically to avoid sulfate salt separation; therefore, models of sulfur solubility are not needed [50]. However, as loading of waste increases, glasses are designed closer to sulfur solubility. Thus, sulfur solubility models have been developed and are used [49,75,95,109].

6.4. Crystalline content at melt temperature

The crystalline content of a glass melt is constrained to avoid plugging the melter pour spout riser [120,121]. Crystals, especially those

containing a high fraction of transition metals, crystallize from the glass-forming melt and tend to exhibit greater densities than the parent melt. Due to the higher densities, these crystalline phases can settle at the bottom of the melter, depending on their size and other factors. Therefore, the crystalline content of a candidate is constrained such that the amount of crystalline phases at 950 °C is < 1 vol% [47,50,121].

Crystallization at temperature is measured according to ASTM Method C1720 [122]. Crushed glass samples are isothermally heat treated in platinum alloy crucibles with tight lids for sufficient time to achieve equilibrium between the melt and crystalline phases [123]. The samples are then quickly cooled to room temperature and analyzed using X-ray diffraction (XRD), light microscopy, and/or scanning electron microscopy to determine the types and quantities of crystals formed.

WTP baseline glasses are designed in a way that avoids crystallization in the melter, so melter crystallization models are not needed [50]. However, enhanced waste glass formulations are designed to optimize waste loading and therefore come closer to property limits. Zirconia-containing phases and cassiterite (SnO_2) tend to form in these glasses at lower temperatures [121]. Crystallization of these phases is primarily controlled by the concentrations of the more refractory components in ILAW glass melts, including Al_2O_3, SnO_2, and ZrO_2, which all increase the tendency to crystallize one of these phases [121], although detailed models have not yet been developed.

6.5. K-3 corrosion

Within the WTP LAW melters, Monofrax™ K-3 refractory is the primary melt-contact refractory (Monofrax™ E refractory is used on some surfaces). Monofrax™ K-3, which is composed of corundum-eskolaite (i.e., Al_2O_3-Cr_2O_3) solid solution and a Mg-Cr-Al-Fe-O spinel phase, is used because of its high electrical resistivity and good corrosion and thermal resistances. To enhance the lifetime of the WTP melters, the glass composition must be designed so that corrosion of K-3 is maintained at a low rate. Some common mechanisms for refractory corrosion in a glass melt include chemical corrosion, physical cracking, spallation/grain pullout, and upward drilling [124,125]. Laboratory-scale methods are used to test K-3 refractory corrosion using a modified ASTM C621 [124,125]. This method uses 1.52 cm × 1.01 cm × 7.62 cm (0.6 in. × 0.4 in. × 3 in.) refractory coupons immersed in a 2.54 cm (1 in.) deep molten glass pool at a fixed temperature for 6 days. After the 6-day test, samples are cooled and bisected for analysis. The thickness at the glass-air interface is reported as the "neck" corrosion [109].

Very limited data are available to project the effect of time and temperature on refractory corrosion. The available data suggest that the corrosion rate significantly increases with temperature and decreases with time [125]. Also, the corrosion is significantly lower along submerged portion of the refractory compared to the melt-air interface (or neck). Due to the lack of data, a conservative constraint on corrosion rate has been adopted: The neck corrosion length of < 1.02 mm (0.04 in) after a 6-day 1208 °C corrosion test with bubbling at 8 cm^3 min^{-1} of air is used [109,124,125]. The 1.02 mm constraint is based on a linear extrapolation of corrosion rate from time = 0–5 years for penetration of the melt through the first 30.5 cm (12 in.) K-3 layer during the melter design life. This constraint is overly conservative because 1) corrosion rates are initially high and then decrease with time to a slow steady-state rate; 2) corrosion rates are based on neck corrosion, which occurs significantly faster than corrosion in the submerged portion of the refractory; 3) the outer wall of the melter is water-cooled, so as corrosion continues to penetrate the refractory, the glass melt will increase in viscosity and ultimately solidify, thereby stopping further corrosion; and 4) the test is performed at 1208 °C while the refractory interface with melt and air will be maintained < 1150 °C [125].

Alkali and alkaline earth components (e.g., Na, Li, Ca, and K) are known to increase the K-3 corrosion while Al, Si, V, Cr, and Cl have been observed to decrease K-3 corrosion [75,109]. The alkali and alkaline earth components attack the Cr_2O_3 and Al_2O_3 constituents of the Monofrax™ refractory, creating an "altered zone" near the interface between the porous refractory and the glass melt [109,126]. Alkali and alkaline earth components also reduce the melt viscosity, which increases material transport away from the refractory surface [109,126]. Chromium is observed to have a clear effect in reducing K-3 corrosion, but Al, Fe, Mg, Ni, and Zn along with Cr have also been observed to form a passivating layer composed of spinel ($A^{2+}B_2^{3+}O_4$, where A and B are divalent or trivalent metals) or nepheline [(Na,K,Ca)(Al,Fe)SiO_4] [109,126]. For high-alkali waste streams, the waste loading is often limited to prevent decreased melter lifetimes [109].

7. Disposal and product performance related constraints

7.1. Disposal in the integrated disposal facility

DOE is planning to dispose of mixed ILAW in the Integrated Disposal Facility (IDF) on the Hanford Site [127]. The IDF is a double-lined, near-surface disposal facility with two isolated disposal cells, one for low-level waste and a second for mixed-low-activity waste that is permitted under the Resource Conservation and Recovery Act (RCRA) by the Washington State Department of Ecology [127]. The mixed waste cell is planned to contain ~130,000 containers of ILAW glass, which makes up ~86% of the volume, where the remaining 14% of the volume will include spent glass melters (~4.5%), solidified secondary liquid waste treatment containers (~5.9%), and WTP solid secondary wastes (~3.7%), see Figure S17 (Supporting Information) for an illustration of the disposal site. Wastes will be emplaced between 15 and 30 m below the surface in layers separated by soil (see Figure S17, Supporting Information). The two cells contain a leachate collection and recovery system composed of a liner and sump. The two cells are identical to one another but are hydraulically separated; water infiltrating each cell flows into separate sumps and is collected in separate leachate recovery tanks. The permit authorizing disposal in the IDF requires a demonstration that the system of engineered and natural features of the disposal facility will limit releases from the facility and be protective of human health and the environment for the next 1000–10,000 years [128]. Post-closure protective features to future members of the public are evaluated after the time of closure and include a 100-year period of institutional controls that limit exposure immediately following closure of the facility [129].

The most recent version of the IDF Performance Assessment (PA) evaluated the dose to a future member of the public that resides or works 100 m from the facility and is exposed to air emissions and groundwater plumes originating at the disposal site [127]. Computer models simulated releases to the atmosphere and to the groundwater and calculated concentrations in the environmental media that result in a dose to the future worker or resident. Using both regulatory-derived and

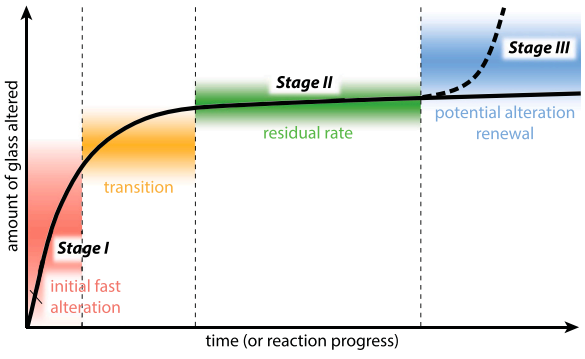

Fig. 8. Diagram showing the general behavior of glass dissolution, which can be described in three major stages. Copyright 2013, American Ceramic Society. This figure was reprinted with permission from Vienna et al. [16].

site-specific exposure factors, doses by inhalation, ingestion, and external exposure were computed and compared to DOE performance objectives in DOE Manual (M) 435.1–1, *Radioactive Waste Management Manual* [129]. Performance objectives included an annual dose limit of 100 μSv yr^{-1} through the air pathway and 250 μSv yr^{-1} from both the air and groundwater pathways. Radon emissions were also calculated and compared to the DOE limit of 0.74 $Bq{\cdot}m^{-2}{\cdot}s^{-1}$ (20 $pCi{\cdot}m^{-2}{\cdot}s^{-1}$). Simulated groundwater concentrations were also compared to national and state water quality standards (e.g., 40 CFR 141) [130]. The IDF PA also evaluated the dose to an inadvertent intruder and compared the resulting dose to performance measures in DOE M 435.1–1 (5 mSv for an acute dose and 1 $mSv{\cdot}yr^{-1}$ for a chronic dose).

ILAW glasses are intended to immobilize long-lived fission products, including ^{99}Tc with a half-life ($t_{1/2}$) of 2.13×10^5 y and ^{129}I with a $t_{1/2}$ of 1.57×10^7 y. Trace amounts of higher activity fission and activation products (e.g., ^{60}Co [$t_{1/2} = 5.271$ y], ^{137}Cs [$t_{1/2} = 30.17$ y], and ^{90}Sr [$t_{1/2} = 29.1$ y]) will also be immobilized in the ILAW glass, but, due to their short half-lives, these isotopes do not significantly impact estimated dose to the maximally exposed individual. Trace concentrations of long-lived actinides are also present (e.g., U isotopes). Integrated system models and process-level models were used to compare doses from ^{129}I and ^{99}Tc to concentrations of other radionuclides (e.g., ^{3}H, ^{60}Co, ^{90}Sr, ^{137}Cs, ^{226}Ra, ^{233}U, ^{234}U, ^{238}U) and hazardous chemicals in a groundwater pathway [131]. The integrated system and process-level models revealed that ^{129}I and ^{99}Tc are the primary dose contributors in the 10,000 years that follow the closure of the IDF [131]. The two primary disposed materials that contribute to estimated dose from the IDF are ILAW glass and secondary solid waste forms (SSW), including encapsulated HEPA filters and other grout-encapsulated debris from the tank waste treatment processes. In the IDF PA, the release of ^{99}Tc from SSW will determine the allowable release of ^{99}Tc over the first 5000 years after the planned closure date of 2051. After approximately 5000 years, glass corrosion rates will determine the release of ^{129}I and ^{99}Tc from IDF [132]. Lysimeter testing of example waste forms in similar site conditions is underway to demonstrate adequate performance [133].

The IDF is constructed but has yet received waste. The IDF is being maintained in pre-operational condition. A surface cover will be installed to reduce infiltration into the facility for 500 years. The engineered surface cover is a sloped surface composed of multiple hydraulic and structural layers intended to promote evapotranspiration, divert water around the facility, and prevent bio-intrusion into the waste zone. The design of this cover is currently only conceptual.

7.2. Glass durability background

Glass is an excellent medium for waste immobilization as it offers compositional flexibility and a high resistance to aqueous attack, referred to as chemical durability. Glass corrosion is a complex process as glass alters at various rates as a function of time and environmental conditions. Much of the ongoing testing for waste forms includes understanding the mechanisms and rates of glass dissolution in the environment over long time periods (i.e., 10^3 to 10^6 y). The dissolution kinetics of alkali-borosilicate glass over time can be described as a function of glass composition, temperature, pH, and solution chemistry [134,135].

The release of high-mobility, long-lived radioisotopes ^{99}Tc and ^{129}I into the vadose zone below IDF is of concern (see Figure S17, Supporting Information). As the radioisotopes (and hazardous components) are chemically bound as part of the glass, the glass must corrode to release them into solution [136–138].

Glass alteration has widely been represented using a kinetic model based on a general rate equation for mineral decomposition based on transition state theory [16,139,140]. For convenience, the rate of glass dissolution can be described in three general stages (Fig. 8). Within the first regime (Stage I), glass alters at its fastest rate. In the second regime (Stage II), glass alteration rates reach a low value due to the formation of a passivating gel layer on the surfaces of the glass and increased concentration of glass components in solution. The third regime (Stage III) is characterized by a sudden increase in the alteration rate. Stage III has only been observed for some glass compositions under a limited set of conditions. For a more rigorous explanation of glass alteration, the reader is directed to recent review articles [16,18,139,140]. The duration and transition times for these stages vary significantly with glass composition and test parameters.

During Stage I, the driving force for dissolution, the difference in chemical potentials among the solution and the glass is high [16,140]. During this stage, alkali species readily exchange with charged species from the solution and the covalently bonded silica glass network undergoes hydrolysis, resulting in the release of orthosilicic acid (H_4SiO_4) [16]. As this stage of alteration progresses, the concentrations of glass components in solution increase while the thermodynamic driving force and alteration rate decrease [16,140]. This deceleration of the alteration rate (given as "transition" in Fig. 8) also coincides with the formation of an "alteration layer" on the surface of the reacting glass, often exemplified as a layer enriched in Si and Al and depleted in alkali and boron. The mechanism for deceleration of the alteration rate is likely a combination of the reduction in driving force and the reduction in mass transport due to the presence of the alteration layer. During Stage II, the glass alteration rate is slow due to the hindered mass transport through the alteration layer and/or the reduced driving force. The alteration layer forms from either condensation of hydrated silica from solution or reconstruction of the hydrolyzed species near the glass surface. Stage III glass alteration has not been observed for all glasses but is characterized by an increase in alteration rate after a prolonged period of a slow alteration. The increase in the rate observed with Stage III behavior is most often concurrent with, and is likely caused by, the precipitation of silicate-containing zeolites and calcium-silicate-hydrate phases [141–143]. Stage III is most often observed in glass corrosion tests with high pH and high temperature [141,142,144,145]. The correlation between zeolites and corrosion acceleration was directly confirmed [143,146].

Accelerated durability assessment methods for alkali-borosilicate glasses were first developed when these materials were adopted as the preferred immobilization matrix for radioactive waste [12,147,148]. The impetus to create standardized test protocols to allow direct comparison of dissolution rates between glasses began in earnest in the early 1980 s and continues today. The timeline for the development of the most commonly used glass dissolution tests over the last four decades is shown in Fig. 9 and an extensive treatment of the subject matter can be found in a recent review by Thorpe et al. [149].

7.3. Current performance assessment rate model

The current IDF PA uses a kinetic model for estimating the alteration rate of glass and thereby the release of isotopes into the environment [150]. This is shown in Eq. (1):

$$r = k_0 a_{H^+}^{-\eta} \exp\left(\frac{-E_a}{RT}\right)\left[1 - \left(\frac{Q}{K_g}\right)\right] \quad (1)$$

where r = the glass dissolution rate (g m^{-2} s^{-1}), k_0 = intrinsic rate constant (g m^{-2} s^{-1}), a_{H+} = hydrogen ion activity, η = pH power coefficient, E_a = apparent activation energy (J mol^{-1}), R = gas constant, 8.314 (J $mol^{-1}{\cdot}K^{-1}$), T = temperature (K), Q = ion-activity product of rate controlling reaction [assumed to be the H_4SiO_4 activity], and K_g = pseudo-equilibrium constant of rate-controlling reaction. Additionally, there is a sodium ion exchange process shown in Eq. (2) that increases solution pH and thereby impacts r:

$$r_{iex} = k_{Na\text{-}H} A \quad (2)$$

where r_{iex} = the sodium ion exchange rate (mol Na s^{-1}), $k_{Na\text{-}H}$ = ion exchange rate constant (mol Na m^{-2} s^{-1}), and A = glass surface area

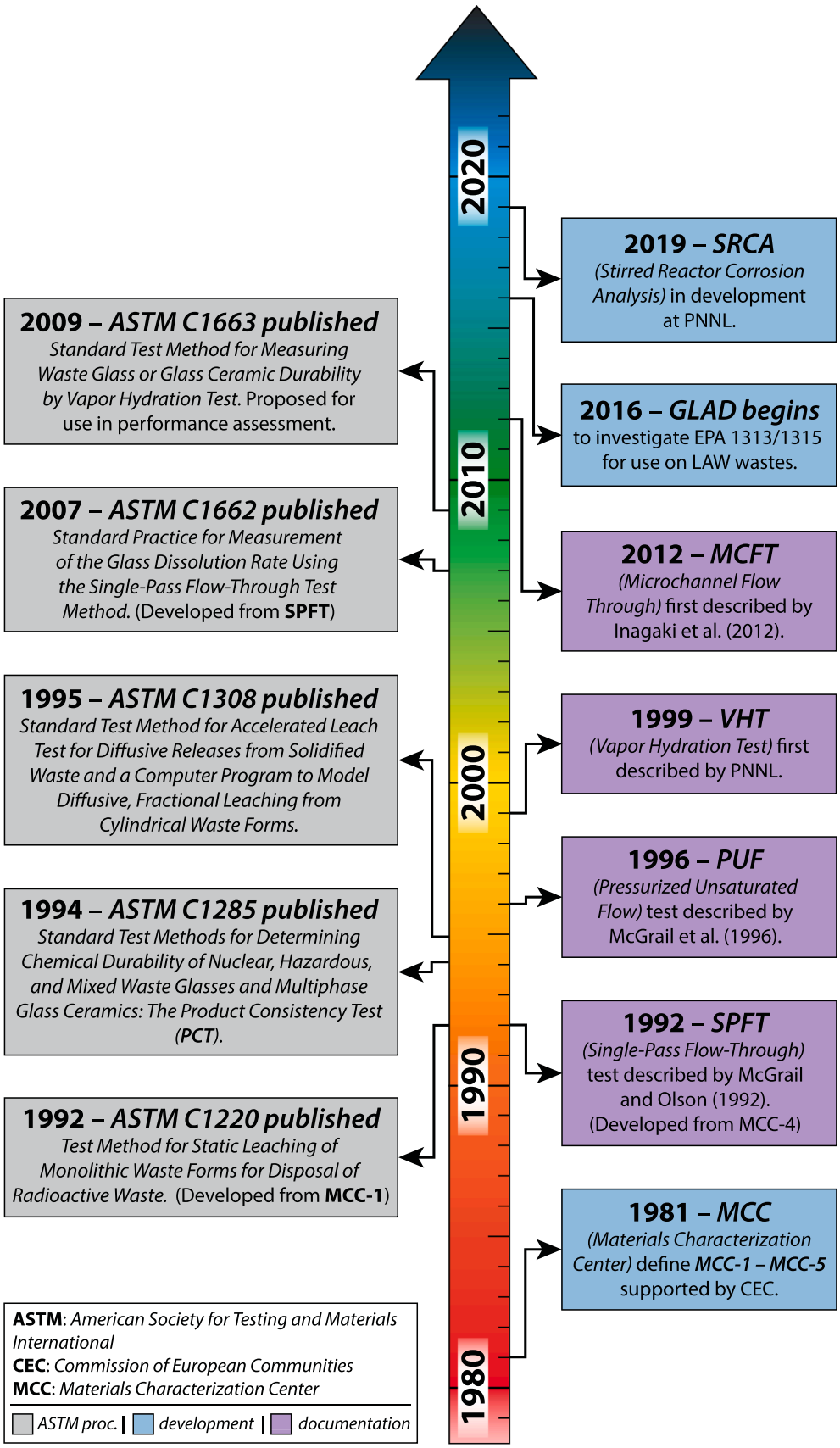

Fig. 9. Timeline showing the development and acceptance of the most commonly used glass durability tests. Modified from the original by Thorpe et al. [149].

(m^2). The model parameters (k_0, η, E_a, K_g, $k_{Na\text{-}H}$) have been measured using single-pass flow through (SPFT) test sequences in which pH, T, and $[H_4SiO_4]$ have been independently and systematically varied [150,151]. K_g is empirically determined using data from SPFT with systematic variation in $[H_4SiO_4]$ or fitted to static corrosion test data. Q is estimated using geochemical model of the solution in contact with glass as function of glass corrosion progress.

In addition to the kinetic portion of the model, a set of equilibrium constants for the secondary phases that act as "sinks" for the ions that control glass affinity is also needed. The set of phases is chosen such that kinetically hindered phases are not included. This set of potential phases is referred to as the reaction network. The phases included in the reaction network are selected using geochemical models to identify possible phases based on solution composition and detailed solids analyses after corrosion under long-duration PCT, VHT, and pressurized unsaturated flowthrough (PUF) tests. The solution progression analyzed in long-duration PCT and PUF has been used to validate reactive transport models of ILAW glass alteration; however, the alteration rates obtained by PCT, VHT, and PUF are not directly used in estimating PA rate parameters. Alternative approaches to estimating the rate of glass alteration in disposal environments are being considered.

7.4. Product consistency test

In general terms, the PCT is performed by immersing glass particles of a controlled particle size in an aqueous solution [75,149,152]. Afterward, the leachate solution is analyzed with ICP-OES to determine the fractions of Na, B, and Si leached into the solution. The fractions of loss or "released" components are normalized to the parent glass composition. PCT method A (PCT-A) is used for ILAW glass qualification, which specifies 90 °C for 7 days with deionized water at a glass-surface-area-to-liquid-volume ratio of roughly 2000 m^{-1} [75,149,152]. The constraint for Hanford ILAW glass PCT response is that the normalized losses (NL_i for i-th species) of Na, B, or Si during the PCT-A be $\leq$ 2 g•m^{-2} [30].

The logarithms of PCT-A normalized Na and B losses have been modeled as functions of composition in order to control the composition of ILAW glass to satisfy the contract requirement. Note that NL_{Si} is always $< NL_B$ and $< NL_{Na}$ and so is not modeled as a function of composition. The components Li, Na, K, Mg, and B have been observed to increase $\ln[NL_B]$ and $\ln[NL_{Na}]$, while the components Al, Si, Ti, Sn, and Zr have been observed to decrease $\ln[NL_B]$ and $\ln[NL_{Na}]$. The components Ca, Fe, V, and Zn have minor effects [72,75,77,88,104].

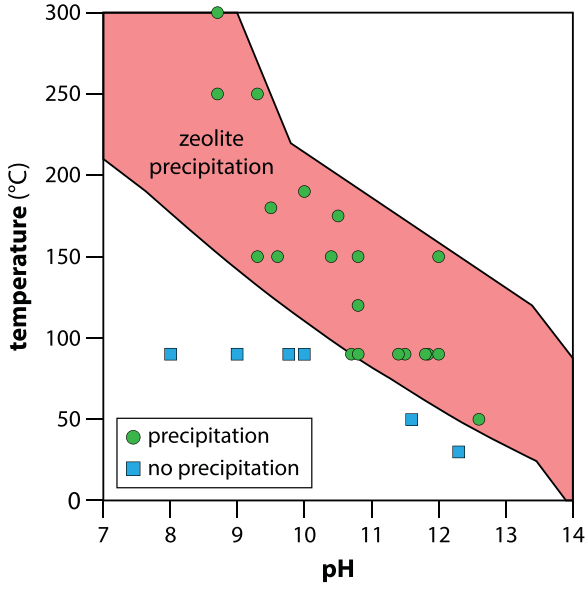

Fig. 10. Stability temperature region for zeolites in glass corrosion solutions vs. pH [166] based on results reported by Zhen-Wu et al. [167] and reprinted with permission from M. Bauchy.

The chemical interpretations for primary component impacts on glass corrosion have been determined. Based on the description of ion exchange, network connectivity, and solution pH in the previous sections, it is intuitive that increasing the fraction of Na, Li, and K in glass will increase the PCT responses [18,75,140]. The effect of boron on increasing the elemental loss may be described by ab initio simulations that estimated that the hydration of B–O–Si and B–O–B linkages exhibits lower reaction energies than Si–O–Si linkages [18,140,153–155]. Aluminum, although generally a network intermediate, is nearly exclusively tetrahedrally coordinated with oxygen in ILAW glasses (i.e., $[AlO_4]^{-5}$). Aluminum requires charge compensation by + 1 to maintain a $[AlO_4]^{-5}$ configuration in glass. As ILAW glasses are generally high in Na_2O concentration, charge compensation is primarily achieved by Na^+, but other alkali or alkaline earth ions may also contribute [18]. Overall, the charge compensation of $[AlO_4]^{-5}$ tetrahedra reduces the number of non-bridging oxygens and polymerizes the melt, which slows water diffusivity [18]. Alkaline earth metal oxides also impact glass corrosion. For example, previous studies by Hrma et al. [156] compared the effect of Ca vs. Mg on glass alteration behavior in different experimental conditions. During testing, Ca was hypothesized to form $CaCO_3$, which would not significantly impact alteration behavior, while Mg formed silicates, which increased the driving force for dissolution and thereby the rate of alteration. Additional researchers have evaluated the differences in effects of CaO vs. MgO on durability [157–160]. Debure et al. [157] found, like Hrma et al. [156] that Mg crystallized as silicates. Aréna et al. [158] and Mercado-Depierre et al. [159] observed Ca uptake in the alteration layer, which is solution-pH dependent. Neeway et al. [161] found that, although Ca reduces short-term corrosion behavior, it may promote Stage III corrosion in the longer-term timescales.

7.5. Vapor hydration test

The VHT is performed by placing a 10 mm × 10 mm × 1.5 mm glass coupon polished to 600 grit (30 μm) within a test vessel with the coupon suspended by a platinum wire. A small amount of deionized water (typically 0.20 g or 200 μL) is added to the bottom of the 304 L stainless steel vessel so that water vapor can interact with the coupon but not reflux during testing at 200 °C [162,163]. The samples are removed from the oven after a predetermined time, then are cross-sectioned and analyzed using optical microscopy and/or electron microscopy to measure the alteration layer thickness, which is then used to calculate the alteration extent in g m^{-2}. The WTP contract specifies that VHT responses performed at 200 °C for $\geq$ 7 days be $<$ 50 g•m^{-2}•d^{-1} [30]. This specification is typically satisfied by measuring r_a of glass samples at a single time (typically 24 days) and estimating the rate as a constant from time = 0. Vienna et al. [164] showed that this method always results in a conservative estimate of the rate obtained from multiple test durations.

The VHT constraint was implemented in the WTP contract in 2000 to help reduce the risk that ILAW glasses would exhibit Stage III behavior during disposal in the IDF. However, the nominal disposal temperature of the IDF is significantly lower than the VHT temperature (15 °C vs. 200 °C). The onset of Stage III behavior, linked to zeolite formation, has been empirically found to be linked to pH and temperature [165]. Bauchy et al. [166,167] found the stability of zeolites to increase with temperature (e.g., becoming stable over lower pH region), and this is shown in Fig. 10. At temperatures near the nominal IDF temperature (15 °C), zeolites are not stable at pH values below 13.5, which are not likely to be experienced in IDF (with maximum estimated pH of 11.5 and nominal values of 8.5) [168]. This implies that the contract constraint adds excessive conservatism.

The effect of composition on logarithm of r_a at 200 °C (and 24 days) has been modeled in addition to the probability of failing the WTP contract VHT specification [72,75,77,88,104,164,169,170]. The

concentrations of Li, Na, and K in the glass have been observed to have a large effect on increasing ln[r_a] while Ti, Zr, Sn, and Si in the glass have been observed to have a large effect in reducing it. Similar trends exist among the components that affect the responses of the PCT and VHT [75].

7.6. Phase changes during container-centerline-cooling

After conversion to a glass melt within the LAW melter, the product is poured into the 304 L stainless steel containers. The large thermal mass of the glass melt (~6 t) causes the melt located near the outer portions of the container to cool rapidly while the glass melt near the center of the container cools slowly. The cooling process for the ILAW container requires roughly 60 h for the container centerline to reach the glass transition temperature [171]. The slow cooling of the glass melt allows for atomic arrangement of the components within the glass melt, potentially resulting in crystallization or liquid-liquid phase separation. This phase separation (either immiscible liquid or crystalline) is a risk because it can degrade the durability of the ILAW glass in unpredictable ways.

A constraint is used to ensure that phase changes do not significantly impact the chemical durability of the final product. One such case is the potential formation of silicate phases that can extract components that enhance the chemical durability of the glass (such as Si), resulting in a residual glass that is enriched in components that reduce the chemical durability (such as Na and B) [172–177].

Liquid-liquid phase separation can occur due to immiscibility of components within a glass-forming melt [178]. Taylor et al. [179] developed an immiscibility model for complex glasses where the composition was simplified to a submixture of Na_2O-B_2O_3-SiO_2, which has a known immiscibility dome. Peeler and Hrma [180] then modified the Taylor submixture model to include the effect of Li_2O, which is more polarizing than Na_2O. The results of Peeler and Hrma [180] most closely matched experimental observations when the mass percent of Li_2O was multiplied by the ratio of the molecular mass of Na_2O/Li_2O then added to the mass percent of Na_2O (to obtain an "equivalent" Na_2O mass percentage) [180]. Similarly, phase separation regions from Li_2O-B_2O_3-SiO_2, A_2O-SiO_2-Al_2O_3-B_2O_3, and (A_2O+AEO)-(SiO_2 +Al_2O_3)-B_2O_3, where AEO = CaO, MgO and M_2O = Na_2O, Li_2O, or K_2O, were compiled by Jantzen et al. [178] and used to generate a composite phase diagram of A_2O-(SiO_2 +Al_2O_3)-B_2O_3, which could be applicable to nuclear waste glasses, Pyrex borosilicate glasses, and VYCOR glasses. An additional model for phase separation was presented by Edwards [181], which utilized statistical discriminant analysis.

To produce quenched and container-centerline-cooled (CCC) samples in the lab, glasses are initially prepared by traditional melt-quenching, where a mixture of additives (e.g., oxides, carbonates, sulfates, chlorides, fluorides) known as a *glass batch* are melted at 1150 °C in 1-hour increments. The glass melt is then poured onto a metal quench plate to solidify. To produce the CCC sample, the quenched material is placed into platinum crucibles and slow cooled from 1150 °C to room temperature following a cooling profile that represents the slowest cooling region in the container – the CCC profile. Crystallization is measured using XRD of both quenched samples and slow-cooled samples. Phase separation can be measured using electron microscopy, small-angle X-ray scattering, or small-angle neutron scattering. Reiser et al. [182] performed ultra-small angle X-ray scattering of glasses designed around the international simple glass composition modified with varying fractions of Al_2O_3. The resulting data matched well with both the Taylor sub-mixture model [179] and the Edwards model [181], but most-closely matched the Edwards model.

7.7. Land disposal restrictions (Disposal)

As Hanford tanks contain RCRA-listed wastes, the ILAW must satisfy land disposal restrictions (LDR). Satisfying LDR typically entails the demonstration that after treatment, the Toxicity Characteristic Leaching Procedure (TCLP) responses of waste satisfy the Universal Treatment Standards [183]. An alternative method is to treat the waste using best demonstrated available technology (BDAT) for a waste type. The treatment standard (BDAT) for HLW is vitrification. However, that treatment standard did not consider all the underlying hazardous constituents (UHC) in Hanford LAW. Therefore, TCLP testing was performed to demonstrate that vitrification sufficiently treated all the UHC in Hanford LAW glasses [184]. These results formed the basis for a Land Disposal Restriction Treatability Variance Petition for Hanford Tank Waste, which extended the high-level waste vitrification (HLVIT) treatment standard to Hanford LAW [185]. The Washington State Department of Ecology has approved the petition under the site-specific variance 40 CFR 268.44(h) [186].

8. Compositional effects summary

As described above, all the chemical components of glass (typically tabulated as either the mass or mole fractions of single metal oxides and halogens) impact glass properties differently. The effects of an individual component on glass and melt properties is generally determined by its bonding nature within the glass/melt. For example, the valence of the element, coordination with oxygen, ionic size, polarizability, and bonding energy have all been shown to correlate with glass property effects in both waste glasses and commercially important glasses. These effects can be simplified using correlations of properties to median crystal bond strength, ion potential, optical basicity, and structural bond strengths, for example [187–196]. Often, the effects of chemical components will improve some properties while making other properties worse. For example, increasing ZrO_2 concentration in glass improves chemical durability but also increases melt viscosity and promotes crystallization. Therefore, glass property-composition models are being developed and used to optimize glass composition to maintain all properties safely within acceptable ranges [36,72,75,197]. Table 4

Table 4
Summary of Component Concentration Effects on ILAW Glass Properties.

Oxide	Al_2O_3	B_2O_3	CaO	Cr_2O_3	Fe_2O_3	K_2O	Li_2O	MgO	Na_2O	SiO_2	SnO_2	TiO_2	ZnO	ZrO_2	Other
Viscosity	↑	↓	↓	↔	↔	↓	↓	↓	↓	↑	↑	↓	↔	↑	–
EC	↔	↔	↔	↔	↔	↑	↑	↔	↑	↓	↔	↔	↔	↔	–
Crystal	↑	↓	↓	↑	↑	↓	↓	↔	↓	↓	↑	↑	↑	↑	NiO, MnO↑
PCT	↓↑	↓↑	↔	↔	↔	↑	↑	↑	↑	↓	↓	↓	↔	↓	–
VHT	↓↑	↓↔	↔	↔	↔	↑	↑	↔↑	↑	↓	↓	↓	↔	↓	–
Nepheline	↑	↓	↑	↔	↔	↑	↑	↔	↑	↓	↔	↔	↔	↔	–
Salt	↑	↓	↓	↑	↔	↓	↓	↔	↓	↑	↔	↔	↔	↔	SO_3, Cl↑, V_2O_5↓
TCLP	↓	↑	↔	↔	↔	↑	↑	↔	↑	↓	↓	↔	↑	↓	–
Corrosion	↓	↔	↔	↓	↓	↑	↑	↔	↑	↓	↓	↔	↓	↓	–

↑ = Increase property; ↓ = Decrease property; ↔ = Small effect on property. Multiple arrows are for non-linear effects; the first is for lower concentrations and the second for higher concentrations. TCLP = toxicity characteristic leaching procedure. Corrosion denotes corrosion of glass contact materials (primarily Monofrax K-3 and Inconel 690).

summarizes the component effects of several oxides on ILAW glass properties.

9. Current glass composition limitations and research prospective

The WTP LAW facility is planned to start operation this year. However, there are potential areas of improvement in glass formulation and process control that have already been identified as discussed earlier in this paper. This section lists some of those improvement opportunities that are currently being pursued.

Lu et al. [36] evaluated the sensitivity of various constraints on loading of Hanford LAW in glass and size of the acceptable glass composition envelope. It was determined that loading was most impacted by three factors: r_a, K-3 corrosion, and process/prediction uncertainties. As described previously, the two constraints that are most limiting (i.e., r_a and K-3 corrosion) are also overly conservative. Efforts are underway to develop new methods to constrain the corrosion of glass-contacting refractories by evaluating the time-temperature-composition-corrosion relationships of K-3 refractory life [125]. The excessive conservatism of the VHT is further exacerbated by the test being performed in a hydrothermal regime with conditions far from those anticipated during disposal. Previous and current research efforts have explored how glass will behave in IDF conditions [168], as well as testing to understand ion exchange behavior [198, 199], secondary phase formation [143,200,201], and glass behavior in dilute conditions [135,202,203].

Durability testing is being performed to 1) quantify the parameters in PA models (SPFT) and 2) control glass composition during production to satisfy durability-related constraints (i.e., PCT and VHT). An ongoing effort is aimed at qualifying results from various standardized tests that 1) are less expensive compared to the SPFT for PA model parameter quantification and at the same time 2) potentially replace the contract-required performance measures with measures directly tied to PA models [149,204,205]. These combined results will be used to improve control of glass composition during production [50,72,73,75] and estimate the final waste form performance in disposal conditions [206].

The UQ method improvements offer significant promise for increasing the size of the ILAW glass processing envelope and the resulting waste loadings. UQ is performed using several approaches. The method currently employed to quantify process uncertainties is based on a Monte Carlo simulation that uses probability distributions for uncertain parameters such as analytical, mixing, sampling, loss to off-gas, GFC composition, and GFC delivery. Modern UQ approaches are being investigated to reduce the range of possible variations by accounting for covariances in process parameters. Additionally, closed form analytical methods will improve the optimization of glass compositions while simultaneously providing confidence in glass compositions and properties. The next largest contributors to uncertainty are property prediction uncertainties, particularly for VHT and PCT responses and sulfur solubility. The currently applied models yield high uncertainty and the total database on which the models are applied is small, particularly near the boundaries of the current constraints. To alleviate these limitations, additional data are being collected at or near the constraints and new model forms are being investigated [75,207–212].

Addressing these three limitations in glass composition and waste loading (r_a, K-3 corrosion, and UQ) will allow for glasses to be processed over a broader range of compositions. Once that is realized, additional data and property-composition models will be needed that cover the newly expanded compositional envelope.

Glass property models to date have been primarily of the form of partial quadratic mixture models (or polynomial functions of glass oxide concentrations). While these forms are well suited to nuclear waste glass design and qualification, they fail to take advantage of recent advances in materials modeling. It is now possible to estimate the molecular structure of multicomponent waste glasses using molecular dynamic simulations [192,213–219]. This will provide an unprecedented ability to perform quantitative structural property relationships [190,191,195]. Additionally, advanced methods in machine learning will enable discovery of new ILAW glass compositions [197,220–223].

Prediction of processing behavior to troubleshoot melter operations has been performed recently using experimental tools in tandem with computational methods [224,225]. In one example, first described by Hrma et al. [226] and then further studied by others [227–229], the melting rate correlation (MRC) equation uses laboratory-scale melting behavior data (volumetric expansion and conversion enthalpy) of melter feeds to predict the glass production rate in a large-scale electric melter. Another example used computational fluid dynamics paired with laboratory-scale diffraction and thermal analysis measurements to predict glass processing rates in prototypical Joule-heated melters and showed reasonable agreement with the MRC and the reported average glass processing rates [225]. Additional measurements are currently being explored that aim to enhance the reliability of these models by using high-temperature X-ray computed tomography and thermal conductivity measurement apparatuses [230–232].

10. Summary and concluding remarks

Over the past several decades, a lot of work has been done within the DOE national laboratory complex and at several U.S. universities to assess management, processing, immobilization, and disposition of the nuclear legacy wastes within the U.S. generated from nuclear weapons production efforts. This paper discusses the specific case of managing Hanford LAW currently stored on the Hanford Site, near Richland, Washington. The scale of the effort to solve these issues at Hanford is immense and will require many more decades to fully realize.

In summary, this paper describes several issues related to management of wastes at Hanford, including the origins of the wastes, the types of waste produced, a summary of the waste treatment processes to be implemented, the glass formulation processes being employed, details about the LAW vitrification technology history, glass property constraints that have to be met for disposal or processing through the melters, as well as the limitations to the current process flowsheet and future directions. The glass property constraints discussed for disposal included product consistency testing, vapor hydration testing, and phase changes during slow cooling. The constraints for processing included viscosity, electrical conductivity, crystalline content at melt temperature, and the K-3 refractory corrosion. Details are provided for all these areas to inform readers and to capture the operation status as of 2023.

The main ongoing research activities on the topic of Hanford LAW relate to 1) improving the processes involved to minimize the waste form production lifecycle and maximize waste loading in the waste forms (which results in fewer containers for disposal) and 2) developing a better understanding other issues like melter (i.e., K-3) corrosion, ILAW glass corrosion, and narrowing down the modeling errors for process and prediction uncertainties. All experimental advances in these areas allow for more processing flexibility that can result in a shorter operation lifetime and with reduced costs to the U.S. government and taxpayers.

Environmental implications

Over 200,000 m^3 of mixed hazardous and radioactive waste is stored in underground tanks at the Hanford site. 56 of 177 tanks are known or suspected of leaking mixed waste to the ground. Plumes of waste are migrating toward the Columbia River. The Waste Treatment and Immobilization Plant is the cornerstone of U.S. Department of Energy's strategy to treat this tank waste and stabilize the radioactive and hazardous constituents of the waste in a stable form for disposal. This paper summarizes over 20 years of development that led to the startup of the worlds largest nuclear waste treatment plant.

Declaration of Competing Interest

The authors declare the following financial interests/personal relationships which may be considered as potential competing interests. John Vienna reports financial support was provided by US Department of Energy. Jose Marcial reports financial support was provided by US Department of Energy. The authors report financial support was provided by US Department of Energy.

Data Availability

Data will be made available on request.

Acknowledgements

This paper is dedicated to Valerie McCain, Waste Treatment and Immobilization Plant (WTP) Project Director (2018–2023), with whom we worked and are fortunate to have known. Valerie was a leader, a coworker, and a colleague in our effort to build and commission the WTP here at Hanford. She was taken from us far too early. Valerie's interactions with us bring to mind the words of Pericles: "What you leave behind is not what is engraved in stone monuments but what is woven into the lives of others." The work summarized in this paper was performed by outstanding contributors, primarily from the Pacific Northwest National Laboratory (PNNL), Bechtel National, Inc., Waste Treatment Completion Company, the Catholic University of America, Duratek (currently Atkins), Savannah River National Laboratory, Washington State University, Rutgers University, Idaho National Laboratory, and many other institutions in the U.K., Czechia, Japan, and France; we thank those contributors for their excellent work and dedication to the success of the WTP. Authors thank Dan Herting of Washington River Protection Solutions for providing images of the tank wastes (Fig. 2). Authors thank Xiaonan Lu (PNNL) for help with Fig. 5. We thank K. Pat Lee (ORANO) for help addressing reviewer questions related to IDF performance assessment. Jim Neeway, Matt Wilburn, and Renee Russell (PNNL) performed reviews of the draft article. Four anonymous reviewers made comments and helpful suggestions that significantly improved this paper. PNNL is operated by the Battelle Memorial Institute for the US Department of Energy (DOE) under contract DE-AC05–76RL01830. This work was funded by the DOE Office of River Protection WTP Project under contract DE-AC05-RL01830.

Associated Content

The Supporting Information is available free of charge. Department of Energy (DOE) documents cited in this paper are available either at the DOE Office of Scientific and Technical Information website (OSTI.gov) or the Hanford Public Reading Room, 2440 Stevens Center Place, MSIN: H6–60, Richland, WA 99354.

Appendix A. Supporting information

Supplementary data associated with this article can be found in the online version at doi:10.1016/j.jhazmat.2023.132437.

References

[1] Bernards, J.K., Hersi, G.A., Hohl, T.M., Jasper, R.T., Mahoney, P.D., Pak, N.K., Reaksecker, S.D., Schubick, A.J., West, E.B., Bergmann, L.M., Golcar, G.R., Praga, A.N., Tilanus, S.N., Crawford, T.W., 2020. River Protection Project System Plan. ORP-11242, Rev. 9. U.S. Department of Energy, Office of River Protection, Richland, WA.

[2] Peterson, R.A., Buck, E.C., Chun, J., Daniel, R.C., Herting, D.L., Ilton, E.S., Lumetta, G.J., Clark, S.B., 2017. Review of the Scientific Understanding of Radioactive Waste at the U.S. DOE Hanford Site. Environ Sci Technol 52, 381–396. https://doi.org/10.1021/acs.est.7b04077.

[3] Gephart, R.E., 2003. A Short History of Hanford Waste Generation, Storage, and Release. PNNL-13605, Rev. 4. Pacific Northwest National Laboratory, Richland, WA.

[4] Gerber, M., 1996. The Plutonium Production Story at the Hanford Site: Processes and Facilities History. WHC-MR-0521. Westinghouse Hanford Company, Richland, WA.

[5] Vienna, J.D., 2010. Nuclear waste vitrification in the United States: recent developments and future options. Int J Appl Glass Sci 1, 309–321. https://doi.org/10.1111/j.2041-1294.2010.00023.x.

[6] Calmus, R.B., 1995. High-Level Waste Melter Alternatives Assessment Report. WHC-EP-0847. Westinghouse Hanford Company, Richland, WA.

[7] Elliott, M., Shafer, P., Lamar, D., Merrill, R., Grunewald, W., Roth, G., Tobie, W., 1996. Hanford High-Level Waste Melter System Evaluation Data Package. PNNL-11016. Pacific Northwest National Laboratory, Richland, WA.

[8] Perez, J., Bickford, D., Day, D., Kim, D., Lambert, S., Marra, S., Peeler, D., Strachan, D., Triplett, M., Vienna, J., Wittman, R., 2001. High-Level Waste Melter Study Report. PNNL-13582. Pacific Northwest National Laboratory, Richland, WA.

[9] Donald, I.W., Metcalfe, B.L., Taylor, R.N.J., 1997. The immobilization of high level radioactive wastes using ceramics and glasses. J Mater Sci 32, 5851–5887. https://doi.org/10.1023/a:1018646507438.

[10] Ojovan, M.I., Lee, W.E., 2011. Glassy wasteforms for nuclear waste immobilization. Metall Mater Trans A 42, 837–851. https://doi.org/10.1007/s11661-010-0525-7.

[11] Hench, L., Charles, R., Cooper, A., Ewing, R., Hutchins, J., Readey, D., Versnyder, F., Wiederhorn, S., 1981. The Evaluation and Review of Alternative Waste Forms for Immobilization of High-Level Radioactive Wastes. USDOE/TIC-11472. U.S. Department of Energy, Office of Nuclear Waste Management, Washington D. C.

[12] Bernadzikowski, T.A., Allender, J.S., Butler, J.L., Gordon, D.E., Gould, J.T.H., Stone, J.A., 1982. Evaluation and Selection of Candidate High-Level Waste Forms. USDOE/TIC-11611. Savannah River Operations Office, Aiken, S. C.

[13] DOE, 1990. Evaluation and Selection of Borosilicate Glass as the Waste Form for Hanford High-Level Radioactive Waste. DOE/RL-90-27. Department of Energy, Richland Operations Office, Richland, WA.

[14] C.M. Jantzen, "Historical development of glass and ceramic waste forms for high level radioactive wastes," pp. 159–172. In *Handbook of Advanced Radioactive Waste Conditioning Technologies*. Edited by M.I. Ojovan, 2011.

[15] Grambow, B., 2006. Nuclear waste glasses - how durable? Elements 2, 357–364. https://doi.org/10.2113/gselements.2.6.357.

[16] Vienna, J.D., Ryan, J.V., Gin, S., Inagaki, Y., 2013. Current Understanding and Remaining Challenges in Modeling Long-Term Degradation of Borosilicate Nuclear Waste Glasses. Int J Appl Glass Sci 4, 283–294. https://doi.org/10.1111/ijag.12050.

[17] Lenting, C., Plümper, O., Kilburn, M., Guagliardo, P., Klinkenberg, M., Geisler, T., 2018. Towards a unifying mechanistic model for silicate glass corrosion. npj Mater Degrad 2, 28. https://doi.org/10.1038/s41529-018-0048-z.

[18] Frankel, G.S., Vienna, J.D., Lian, J., Guo, X., Gin, S., Kim, S.H., Du, J., Ryan, J.V., Wang, J., Windl, W., Taylor, C.D., Scully, J.R., 2021. Recent advances in corrosion science applicable to disposal of high-level nuclear waste. Chem Rev 121, 12327–12383. https://doi.org/10.1021/acs.chemrev.0c00990.

[19] Verney-Carron, A., Gin, S., Libourel, G., 2010. Archaeological analogs and the future of nuclear waste glass. J Nucl Mater 406, 365–370. https://doi.org/10.1016/j.jnucmat.2010.09.028.

[20] Eliassen, R., Goldman, M., 1959. Disposal of High-Level Wastes by Fixation in Fused Ceramics. In: Hearings on Industrial Radioactive Waste Disposal, Vol. 3. Government Printing Office, pp. 1966–1979.

[21] Lutze, W., Ewing, R.C., 1988. Radioactive Waste Forms for the Future. 0444871047. North-Holland.

[22] Ojovan, M., Lee, W., 2005. An Introduction to Nuclear Waste Immobilization. Elsevier, Oxford, U.K.

[23] Agnew, S.F., Boyer, J., Corbin, R.A., Duran, T.B., Fitzpatrick, J.R., Jurgensen, K. A., Ortiz, T.P., Young, B.L., 1997. Hanford Tank Chemical and Radionuclide Inventories: HDW Model. LA-UR-96-3860, Rev. 4. Los Alamos National Laboratory, Los Alamos, NM.

[24] Anderson, J.D., 1990. A History of the 200 Area Tank Farms. WHC-MR-0132. Westinghouse Hanford Company, Richland, WA.

[25] Brevick, C.H., Funk, J.W., Newell, R.L., 1996. Historical Tank Content Estimate Report for the Northeast Quadrant of the Hanford 200 East Area. HNF-SD-WM-ER-349, Rev. 1. Westinghouse Hanford Company, Richland, WA.

[26] Brevick, C.H., Stroup, J.L., Funk, J.W., 1997. Historical Tank Content Estimate for the Southeast Quadrant of the Hanford 200 Areas. HNF-SD-WM-ER-350, Rev. 1. Fluor Daniel Northwest, Inc., Richland, WA.

[27] Brevick, C.H., Stroup, J.L., Funk, J.W., 1997. Historical Tank Content Estimate for the Northwest Quadrant of the Hanford 200 West Area. HNF-SD-WM-ER-351, Rev. 1. Fluor Daniel Northwest, Inc., Richland, WA.

[28] Brevick, C.H., Stroup, J.L., Funk, J.W., 1997. Historical Tank Content Estimate for the Southwest Quadrant of the Hanford 200 West Area. HNF-SD-WM-ER-352, Rev. 1. Fluor Daniel Northwest, Inc., Richland, WA.

[29] Best Basis Inventory, https://phoenix.pnnl.gov/phoenix/apps/gallery/index.html, 2023.

[30] DOE, Contract DE-AC27–01RV14136 (as amended), U.S. Department of Energy, Office of River Protection, Richland, WA, 2001.

[31] DOE, 2013. Hanford Tank Waste Retrieval, Treatment, and Disposition Framework. U.S. Department of Energy, Washington, D.C.

[32] R. Raymond, R. Powell, D. Hamilton, W. Kitchen, B. Mauss, T. Brouns, Initial Selection of Supplemental Treatment Technologies for Hanford's Low-Activity Tank Waste, pp. 21 (WM-4524), Proc. of Waste Management 2004 Symposium Proceeding: HLW, LLW, Mixed, Hazardous Wastes and Environmental Restoration - Working Towards a Cleaner Environment, 2004.

[33] Mann, F., Mcgrail, B., Bacon, D., Serne, R., Krupka, K., Puigh, R., Khaleel, R., Finfrock, S., 2003. Risk Assessment Supporting the Decision on the Initial Selection of Supplemental ILAW Technologies. RPP-17675. CH2MHill Hanford Group, Richland, WA.

[34] NAS, National Academies of Sciences, Engineering, and Medicine, Washington, D. C., 2022.

[35] Westesen, A.M., Campbell, E.L., Fiskum, S.K., Carney, A.M., Trang-Le, T.T., Peterson, R.A., 2022. Impact of feed variability on cesium removal with multiple actual waste samples from the Hanford site. Sep Sci Technol 57, 2482–2490. https://doi.org/10.1080/01496395.2022.2059378.

[36] Lu, X., Kim, D.S., Vienna, J.D., 2021. Impacts of constraints and uncertainties on projected amount of Hanford low-activity waste glasses. Nucl Eng Des 385, 111543. https://doi.org/10.1016/j.nucengdes.2021.111543.

[37] Mears, D., 2018. LAB Facility Design Description. 24590-LAB-3ZD-60-00003, Rev. 2. River Protection Project, Waste Treatment Plant, Richland, WA.

[38] Townsend, P., 2020. Low-Activity Waste Melter Process (LMP) System Design Description. 24590-LAW-3ZD-LMP-00001, Rev. 4, ORP-69026. DOE Office of River Protection, Richland WA.

[39] K.S. Matlack, H. Abramowitz, I. Muller, I. Joseph, I.L. Pegg. 2022. DFLAW Glass and Feed Qualifications for AP-107 to Support WTP Start-Up and Flow-Sheet Development (VSL-18R4500–1, Rev 0). ORP-67601. Vitreous State Laboratory of The Catholic University of America, Washington, D.C.

[40] Matlack, K.S., Kruger, A.A., Gong, W., Bardakci, T., D'Angelo, N.A., Kot, W.K., Pegg, I.L., 2011. Integrated DM1200 Melter Testing of HLW C-106/AY-102 Composition Using Bubblers. VSL-03R3800-1, ORP-51439 Rev. 0. Vitreous State Laboratory, The Catholic University of America, Washington, D.C.

[41] Hamel, W., Sheridan, M., Valenti, P., 1988. Vitrification at the west valley demonstration project. Radio Mag 27–40.

[42] L. Petkus, J. Paul, P. Valenti, H. Houston, J. May, A complete history of the high-level waste plant at the West Valley Demonstration Project, pp. 244, Proc. of Waste Management, 2003.

[43] Chapman, C., Drosjack, W., 1988. Vitrification Process Equiptment Design for the West Valley Demonstration Project. DOE/NE/44139-42. West Valley Nuclear Services Co., West Valley, NY.

[44] Pope, J.M., Macias, D., 1998. Success with the Largest Vitrification of Low-Level Mixed Waste. Institute of Nuclear Materials Management, Mount Laurel, NJ.

[45] M.R. Norton, H.B. Shah, M.E. Stone, L. Johnson, R. O'Driscoll, Overview - Defense Waste Processing Facility opeprating experience, pp. 1–13, Proc. of Waste Management, 2002.

[46] J.M. Perez, Practical and Historical Bases for a Glass Viscosity Range for Joule-Heater Ceramic Melter Operation, personal correspondence, CCN: 150054, 2006.

[47] K. Clarke. 2003. Engineering Specification for Low Activity Waste Melters. 24590-LAW-3PS-AE00-T0001, Rev. 2. River Protection Project, Waste Treatment Plant, Richland WA.

[48] I. Muller, H. Gan, K. Gilbo, I. Pegg, I. Joseph. 2015. LAW Glass Property-Composition Models for K-3 Refractory Corrosion and Sulfate Solubility. VSL-15R3270–1. Vitreous State Laboratory, the Catholic University of America, Washington, D.C.

[49] Vienna, J., Kim, D., Muller, I., Piepel, G., Kruger, A., 2014. Toward understanding the effect of low-activity waste glass composition on sulfur solubility. J Am Ceram Soc 97, 3135–3142. https://doi.org/10.1111/jace.13125.

[50] D.S. Kim, J.D. Vienna 2012. Preliminary ILAW Formulation Algorithm Description, 24590 LAW RPT-RT-04–0003, Rev. 1. ORP-56321. Office of River Protection, Richland, WA.

[51] C. Wilson, K. Burgard, E. Weber, N. Brown, Melter Technology Evaluation for Vitrification of Hanford Site Low-Level Waste, pp. WHC-SA-2857-FP; CONF-950401–950423, Proc. of Am. Ceram. Soc. Cincinnati, OH, 1995.

[52] D. Kim, P. Hrma, S. Palmer, D. Smith, M. Schweiger, Effect of B_2O_3, CaO, and Al_2O_3 on the Chemical Durability of Silicate Glasses for Hanford Low-Level Waste Immobilization, pp. 531–538, Proc. of Environmental Issues and Waste Management Technologies, Ceramic Transactions, 61. Westerville, OH, 1995.

[53] Feng, X., Hrma, P., Westsik, J., JH, Brown, N., Schweiger, M., Li, H., Vienna, J., Chen, G., Piepel, G., Smith, D., McGrail, B., Palmer, S., Kim, D., Peng, Y., Hahn, W., Bakel, A., Ebert, W., Peeler, D., Chang, C., 1996. Glass Optimization for Vitrification of Hanford Site Low-Level Tank Waste. PNNL-10918. Pacific Northwest Laboratory, Richland, WA.

[54] W. Ramsey, M. Gray, R. Calmus, J. Edge, B. Garrett, Next Generation Melters for Vitrification of Hanford Wastes: Status and Direction, pp. 11049, Proc. of Waste Management. Phoenix, AZ, 2011.

[55] NASEM, Review of the Final Draft Analysis of Supplemental Treatment Approaches of Low-Activity Waste at the Hanford Nuclear Reservation: Review #3. 978–0-309–49521-9. Washington, D.C.: The National Academies Press, National Academies of Sciences, Engineering, and Medicine (2019).

[56] Jantzen, C.M., Pierce, E.M., Bannochie, C.J., Burket, P.R., Cozzi, A.D., Crawford, C.L., Daniel, W.E., Fox, K.M., Herman, C.C., Miller, D.H., Missimer, D. M., Nash, C.A., Williams, M.F., Brown, C.F., Qafoku, N.P., Neeway, J.J., Valenta, M.M., Gill, G.A., Swanberg, D.J., Robbins, R.A., Thompson, L.E., 2015. Fluidized Bed Steam Reformed Mineral Waste Form Performance Testing to Support Hanford Supplemental Low Activity Waste Immobilization Technology Selection. SRNL-STI-2011-00387. Savannah River National Laboratory, Aiken, SC.

[57] Jantzen, C., 2008. Mineralization of Radioactive Wastes by Fluidized Bed Steam Reforming (FBSR): Comparisons to Vitreous Waste Forms, and Pertinent Durability Testing. WSRC-STI-2008-00268. Savannah River National Laboratory, Aiken, SC.

[58] J. Wilson, J. Garfield, J. Luey, Design of the Demonstration Bulk Vitrification System for the Supplemental Treatment of Low Activity Tank Waste at Hanford, pp. WM-8310, Proc. of Waste Management. Phoenix, AZ, 2008.

[59] K. Witwer, E. Dysland, J. Garfield, T. Beck, J. Matyas, L. Bagaasen, S. Cooley, E. Pierce, D.-S. Kim, M. Schweiger, Hanford's Supplemental Treatment Project: Full-Scale Integrated Testing of In-Container-Vitrification and a 10,000-Liter Dryer, Proc. of Waste Management. Phoenix, AZ, 2008.

[60] Ard, K., 2011. Bulk Vitrification Technology for the Treatment and Immobilization of Low-Activity Waste. RPP-48703. Washington River Protection Solutions, Richland, WA.

[61] Skeen, R.S., Langston, C.A., McCabe, D.J., Nash, C.A., Asmussen, R.M., Saslow, S. A., Pegg, I.L., Miskho, A.G., 2020. Evaluation of Technologies for Enhancing Grout for Immobilizing Hanford Supplemental Low-Activity Waste (SLAW). SRNL-STI-2020-00228. Savannah River National Laboratory, Aiken, SC.

[62] Muller, I., Pegg, I., Buechele, A., Gan, H., Kim, C., Lai, S., Del Rosario, G., Yan, Q., 1998. Formulation and Testing with TWRS LAW Simulants. ORP-56328. Vitreous State Laboratory, The Catholic University of America, Washington, D.C.

[63] Measurement Of The Leachability Of Solidified Low-Level Radioactive Wastes By A Short-Term Test Procedure, ANSI-16.1, American Nuclear Society, La Grange Park, IL, 2019.

[64] Muller, I., Pegg, I., 2003. Baseline LAW Glass Formulation Testing. VSL-03R3460-1, ORP-55237. Vitreous State Laboratory, The Catholic University of America, Washington, D.C.

[65] Gimpel, R., 2002. WTP Calculation Sheet: Determining the LAW Glass Former Constituents and Amounts for G2 and ACM Models. 24590-LAW-M4C-LFP-00002, Rev. B, ORP-56511. River Protection Project, Waste Treatment Plant, Richland, WA.

[66] Muller, I., Diener, G., Joseph, I., Pegg, I., 2004. Proposed Approach for Development of LAW Glass Formulation Correlation. VSL-04L4460-1, Rev. 2, ORP-56326. Vitreous State Laboratory, The Catholic University of America, Washington, D.C.

[67] Diener, G., 2004. RPP-WTP LAW Pilot Melter Test Summary Report. TRR-PLT-027, Rev. 0. Duratek, Inc, Columbia, MD.

[68] Hamel, W., Holton, L., Demick, L., 2003. An Assessment of the Factors Affecting the Ability to Increase the Na_2O Loading in the Waste Treatment and Immobilization Plant (WTP) Low-Activity Waste (LAW) Glass. ORP-68871. US Department of Energy, Office of River Protection, Richland, WA.

[69] Vienna, J., Schweiger, M., Smith, D., Smith, H., Crum, J., Peeler, D., Reamer, I., Musick, C., Tillotson, R., 1999. Glass Formulation Development for INEEL Sodium-Bearing Waste. PNNL-12234. Pacific Northwest National Laboratory, Richland, WA.

[70] Darab, J., Graham, D., Macissac, B., Russell, R., Smith, H., Vienna, J., Peeler, D., 2001. Sulfur Partitioning During Vitrification of INEEL Sodium Bearing Waste: Status Report. PNNL-13588. Pacific Northwest National Laboratory, Richland, WA.

[71] Peeler, D., Edwards, T., Reamer, I., Workman, P., Vienna, J., Crum, J., Schweiger, M., 2001. Glass Formulation Development for INEEL Sodium-Bearing Waste (WM-180) (U). WSRC-TR-2001-00295. Westinghouse Savannah River Company, Aiken, SC.

[72] J. Vienna, G. Piepel, D. Kim, J. Crum, C. Lonergan, B. Stanfill, B. Riley, S. Cooley, T. Jin, 2016. Update of Hanford Glass Property Models and Constraints for Use in Estimating the Glass Mass to Be Produced at Hanford by Implementing Current Enhanced Glass Formulation Efforts. PNNL-25835. Pacific Northwest National Laboratory, Richland, WA.

[73] Lumetta, N., Kim, D., Vienna, J., 2020. Preliminary Enhanced LAW Glass Formulation Algorithm. PNNL-29475. Pacific Northwest National Laboratory, Richland, WA.

[74] Muller, I., Matlack, K., Gan, H., Pegg, I., 2019. . Optimization of Enhanced LAW Correlation Glasses for Processing. VSL-19R4460-1. Vitreous State Laboratory, The Catholic University of America, Washington, D.C.

[75] Vienna, J., Heredia-Langner, A., Cooley, S., Holmes, A., Kim, D., Lumetta, N., 2022. Glass Property-Composition Models for Support of Hanford WTP LAW Facility Operation. PNNL-30932, Rev. 2. Pacific Northwest National Laboratory, Richland, WA.

[76] Lumetta, N., Kim, D., Vienna, J., 2023. Preliminary Enhanced LAW Glass Formulation Algorithm. PNNL-29475, Rev. 2. Pacific Northwest National Laboratory, Richland, WA.

[77] J. Vienna, D. Kim, D. Skorski, J. Matyas, 2013. Glass Property Models and Constraints for Estimating the Glass to Be Produced at Hanford by Implementing Current Advanced Glass Formulation Efforts. PNNL-22631, Rev. 1, ORP-58289. Pacific Northwest National Laboratory, Richland, WA.

[78] Lumetta, N., Kim, D., Vienna, J., 2022. Preliminary Enhanced LAW Glass Formulation Algorithm. PNNL-29475, Rev. 1. Pacific Northwest National Laboratory, Richland, WA.

[79] B. Rieck, A. Kelly, P. Benson, Software Prototyping of the WTP Immobilized LAW Formulation Algorithm, pp. 18457, Proc. of Waste Management 2018. Phoenix, AZ, 2018.

[80] Rieck, B., 2019. LAW Glass App Design Description. 24590-WTP-PASW-PENG-17-00013-04. Rev. 1. River Protection Project, Waste Treatment Plant, Richland, WA.

[81] Lee, S., Ferkl, P., Pokorny, R., Klouzek, J., Hrma, P., Eaton, W., Kruger, A., 2020. Simplified melting rate correlation for radioactive waste vitrification in electric furnaces. J Am Ceram Soc 103, 5573–5578. https://doi.org/10.1111/jace.17281.

[82] Heredia-Langner, A., Gervasio, V., Cooley, S., Lonergan, C., Kim, D., Kruger, A., Vienna, J., 2022. Hanford low-activity waste glass melts composition-temperature-viscosity relationships. Int J Appl Glass Sci 13, 514–525. https://doi.org/10.1111/ijag.16580.

[83] ASTM C965–96(2017), Standard Practice for Measuring Viscosity of Glass Above the Softening Point, American Society for Testing and Materials International, 2017.

[84] Hrma, P., Arrigoni, B., Schweiger, M., 2009. Viscosity of many-component glasses. J Non-Cryst Solids 355, 891–902. https://doi.org/10.1016/j.jnoncrysol.2009.03.005.

[85] Hrma, P., 2008. Arrhenius model for high-temperature glass-viscosity with a constant pre-exponential factor. J Non-Cryst Solids 354, 1962–1968. https://doi.org/10.1016/j.jnoncrysol.2007.11.016.

[86] Hrma, P., Han, S., 2012. Effect of glass composition on activation energy of viscosity in glass-melting-temperature range. J Non-Cryst Solids 358, 1818–1829. https://doi.org/10.1016/j.jnoncrysol.2012.05.030.

[87] Hrma, P., Kruger, A., 2016. High-temperature viscosity of many-component glass melts. J Non-Cryst Solids 437, 17–25. https://doi.org/10.1016/j.jnoncrysol.2016.01.007.

[88] J. Vienna, D. Kim, P. Hrma, 2002. Database and Interim Glass Property Models for Hanford HLW and LAW Glasses. PNNL-14060. Pacific Northwest National Laboratory, Richland, WA.

[89] Hrma, P., Piepel, G., Redgate, P., Smith, D., Schweiger, M., Vienna, J., Kim, D.-S., 1995. Prediction of processing properties for nuclear waste glasses. Proc Ceram Trans 61, 505–513.

[90] Vienna, J., Hrma, P., Kim, D.-S., Schweiger, M., Smith, D., 1996. Compositional dependence of viscosity, electrical conductivity, and liquidus temperature of multicomponent borosilicate waste glasses. Proc Ceram Trans 72, 427–436.

[91] Piepel, G., Heredia-Langner, A., Cooley, S., 2008. Property-composition-temperature modeling of waste glass melt data subject to a randomization restriction. J Am Ceram Soc 91, 3222–3228. https://doi.org/10.1111/j.1551-2916.2008.02590.x.

[92] Ferkl, P., Hrma, P., Kruger, A., 2022. Parsimonious viscosity-composition relationships for high-temperature multicomponent glass melts. J Asian Ceram Soc 10, 83–98. https://doi.org/10.1080/21870764.2021.2012903.

[93] Hrma, P., Ferkl, P., Kruger, A.A., 2022. Glass length: workability and meltability of glass as a function of glass melt fragility. J Non-Cryst Solids 597, 121931. https://doi.org/10.1016/j.jnoncrysol.2022.121931.

[94] Dietzel, A., 1942. Die Kationenfeldstärken und ihre Beziehungen zu Entglasungsvorgängen, zur Verbindungsbildung und zu den Schmelzpunkten von Silicaten. Z Eleckrochem 48, 9–23. https://doi.org/10.1002/bbpc.19420480104.

[95] Bingham, P.A., Vaishnav, S., Forder, S.D., Scrimshire, A., Jaganathan, B., Rohini, J., Marra, J.C., Fox, K.M., Pierce, E.M., Workman, P., Vienna, J.D., 2017. Modelling the sulfate capacity of simulated radioactive waste borosilicate glasses. J Alloy Compd 695, 656–667. https://doi.org/10.1016/j.jallcom.2016.11.110.

[96] Cassar, D., 2021. ViscNet: neural network for predicting the fragility index and the temperature-dependency of viscosity. Acta Mater 206, 116602. https://doi.org/10.1016/j.actamat.2020.116602.

[97] Mauro, J.C., Yue, Y., Ellison, A.J., Gupta, P.K., Allan, D.C., 2009. Viscosity of glass-forming liquids. Proc Natl Acad Sci 106, 19780–19784. https://doi.org/10.1073/pnas.0911705106.

[98] Vogel, H., 1921. Das Temperaturabhaengigkeitsgesetz der Viskositaet von Fluessigkeiten [The temperature-dependent viscosity law for liquids]. Phys Z 22, 645.

[99] Tammann, G., Hesse, W., 1926. Die Abhängigkeit der Viscosität von der Temperatur bie unterkühlten Flüssigkeiten [The dependence of viscosity on temperature in supercooled liquids]. Z Anorg Allg Chem 156, 245–257. https://doi.org/10.1002/zaac.19261560121.

[100] Fulcher, G.S., 1925. Analysis of recent measurements of the viscosity of glasses. J Am Ceram Soc 8, 339–355. https://doi.org/10.1111/j.1151-2916.1925.tb16731.x.

[101] Gan, H., Buechele, A.C., Kim, C.W., Huang, X., Mohr, R.K., Pegg, I.L., 1999. Corrosion of inconel-690 electrodes in waste glass melts. Proc MRS Online Proc Libr 556, 287.

[102] Careem, M., Mellander, B., 1985. Electrical conductivity of Na_2SO_4(I). Solid State Ion 15, 327–330. https://doi.org/10.1016/0167-2738(85)90136-5.

[103] Ehrt, D., Keding, R., 2009. Electrical conductivity and viscosity of borosilicate glasses and melts, Eur. J. Glass Sci. Technol. B. Phys Chem Glass 50, 165–171.

[104] Piepel, G., Cooley, S., Muller, I., Gan, H., Joseph, I., Pegg, I., 2007. ILAW PCT, VHT, Viscosity, and Electrical Conductivity Model Development: VSL-07R1230-1. ORP-56502. Vitreous State Laboratory, The Catholic University of America, Washington, D.C.

[105] Muller, I., Gan, H., Buechele, A., Pegg, I., 2002. Enhanced K-3 Refractory Corrosion with LAW AZ-102 Glass Formulations. VSL-02S4600-1. Catholic University of America, Washington, D.C.

[106] Gan, H., Feng, Z., Chaudhuri, M., Xie, X., Pegg, I., Joseph, I., 2017. Corrosion Testing of Inconel and K-3 in LAW Glass. VSL-17R4240-1. The Catholic University of America, Washington, D.C.

[107] Skidmore, C., Vienna, J., Jin, T., Kim, D., Stanfill, B., Fox, K., Kruger, A., 2019. Sulfur Solubility in Low Activity Waste Glass and Its Correlation to Melter Tolerance. Int J Appl Glass Sci 10, 558–568. https://doi.org/10.1111/IJAG.13272.

[108] McKeown, D.A., Muller, I.S., Matlack, K.S., Pegg, I.L., 2002. X-ray absorption studies of vanadium valence and local environment in borosilicate waste glasses using vanadium sulfide, silicate, and oxide standards. J Non-Cryst Solids 298, 160–175. https://doi.org/10.1016/S0022-3093(02)00945-6.

[109] Muller, I.S., Gilbo, K., Chaudhuri, M., Pegg, I.L., Joseph, I., 2018. K-3 Refractory Corrosion and Sulfate Solubility Model Enhancement. ORP-63490. VSL-18R4360-1. Vitreous State Laboratory, The Catholic University of America, Washington, DC.

[110] Xu, X., Han, T., Huang, J., Kruger, A.A., Kumar, A., Goel, A., 2021. Machine Learning Enabled Models to Predict Sulfur Solubility in Nuclear Waste Glasses. ACS Appl Mater Interfaces 13, 53375–53387. https://doi.org/10.1021/acsami.1c10359.

[111] Stefanovskii, S.V., Lifanov, F.A., 1989. Glasses for immobilisation of sulfate-containing radioactive wastes. Radiokhimiya 31, 746–751.

[112] S.V. Stefanovskii, 1993. Immobilization of sulfate-containing radiative wastes in glass, Phys. Chem. Mater. Proc. (Fizika i Khimiya Obrabotki Materialov) 63–77.

[113] Manara, D., Grandjean, A., Pinet, O., Dussossoy, J.L., Neuville, D.R., 2007. Sulfur behavior in silicate glasses and melts: implications for sulfate incorporation in nuclear waste glasses as a function of alkali cation and V_2O_5 content. J Non-Cryst Solids 353, 12–23. https://doi.org/10.1016/j.jnoncrysol.2006.09.041.

[114] Jin, T., Skidmore, C.H., Kruger, A.A., Vienna, J.D., 2022. Impacts of temperature on sulfur solubility in low-activity waste glasses. Int J Appl Glass Sci 13, 244–253. https://doi.org/10.1111/ijag.16550.

[115] Goles, R.W., Perez, J.M., MacIsaac, B.D., Siemer, D.D., McCray, J.A., 2001. Test Summary Report INEEL Sodium-Bearing Waste Vitrification Demonstration RSM-01-1. PNNL-13522. Pacific Northwest National Laboratory, Richland, WA.

[116] Goldman, D., 1985. Redox and Sulfur Solubility in Glass Melts. In International Congress on Glass. Charleroi, Belgium.

[117] Schreiber, H., Kozak, S., Leonhard, P., 1985. Sulfur chemistry in a glass-forming borosilicate melt. Am Ceram Soc Bull 64, 1339-1339.

[118] Schreiber, H., Kozak, S., Leonhard, P., McManus, K., 1987. Sulfur chemistry in a borosilicate melt: part 1. redox equilibria and solubility. Glass Sci Technol 60, 389–398.

[119] Schreiber, H., Kozak, S., Leonhard, P., McManus, K., Schreiber, C., 1988. Sulfur chemistry in a borosilicate melt: part 2. kinetic-properties. Glass Sci Technol 61, 5–11.

[120] Lonergan, C.E., Akinloye-Brown, K., Rice, J., Gervasio, V., Canfield, N., Schweiger, M.J., Vienna, J.D., 2019. Micron-sized spinel crystals in high level waste glass compositions: Determination of crystal size and crystal fraction. J Nucl Mater 514, 196–207. https://doi.org/10.1016/j.jnucmat.2018.11.039.

[121] Lonergan, C., Lu, X., Baird, S., Sannoh, S., Vienna, J., 2022. Glass Crystallization Constraints for WTP LAW Operations: Assessment of Isothermal Treatments on Crystal Formation. PNNL-31334. Rev. 1. Pacific Northwest National Laboratory, Richland, WA.

[122] ASTM C1720–11, Standard Test Method for Determining Liquidus Temperature of Immobilized Waste Glasses and Simulated Waste Glasses, American Society for Testing and Materials International, 2011.

[123] Riley, B.J., Hrma, P.R., Vienna, J.D., Schweiger, M.J., Rodriguez, C.P., Crum, J.V., Lang, J.B., Marra, J.C., Johnson, F.C., Peeler, D.K., Leonelli, C., Ferrari, A.M., Lancellotti, I., Dussossoy, J.-L., Hand, R.J., Schofield, J.M., Connelly, A.J., Short, R., Harrison, M.T., 2011. The liquidus temperature of nuclear waste glasses: an international round-robin study. Int J Appl Glass Sci 2, 321–333. https://doi.org/10.1111/j.2041-1294.2011.00063.x.

[124] Pecoraro, G., 2005. "How the Properties of Glass Melts Influence the Dissolution of Refractory Materials,". In: Pye, L., Montenero, A., Joseph, I. (Eds.), In Properties of Glass-Forming Melts. CRC Press, p. 339.

[125] Jin, T., Hall, M., Vienna, J., Eaton, W., Amoroso, J., Wiersma, B., Li, W., Abboud, A., Guillen, D., Kruger, A., 2023. Glass-contact refractory of the nuclear waste vitrification melters in the united states: a review of corrosion data and melter life. Int Mater Rev. https://doi.org/10.1080/09506608.2023.2211469.

[126] Smith-Gray, N.J., Bussey, J.M., McCloy, J.S., 2022. Microstructural examination of interactions between chromia-based refractory and nuclear glass in a melter. J Am Ceram Soc 105, 7760–7769. https://doi.org/10.1111/jace.18706.

[127] WRPS. 2018. Performance Assessment for the Integrated Disposal Facility, Hanford Site, Washington. RPP-RPT-59958, Rev. 1. Washington River Protection Solutions, Richland, WA.

[128] DOE, DOE-STD-5002–2017, 2017.

[129] DOE, 2007. Radioactive Waste Management Manual. DOE M 435.1-1. U.S. Department of Energy, Washington, D.C.

[130] National Primary Drinking Water Regulations, Subpart G—National Primary Drinking Water Regulations: Maximum Contaminant Levels and Maximum Residual Disinfectant Levels, §141.66 Maximum contaminant levels for radionuclides (Code of Federal Regulations), 40 CFR 141, National Primary Drinking Water Regulations, Subpart G—National Primary Drinking Water Regulations: Maximum Contaminant Levels and Maximum Residual Disinfectant Levels, §141.66 Maximum contaminant levels for radionuclides (Code of Federal Regulations), Environmental Protection Agency, Washington, D.C.,

[131] Lee, K., 2018. System Model Calculations for the Integrated Disposal Facility Performance Assessment, Rev. 1A. RPP-CALC-61194. INTERA, Inc. for Washington River Protection Solutions, LLC, Richland, WA.

[132] WRPS, 2019. Performance Assessment for the Integrated Disposal Facility, Hanford Site, Washington. RPP-RPT-59958, Rev. 1A. Washington River Protection Solutions, Richland, WA.

[133] Meyer, P., Asmussen, R., Neeway, J.J., Thomle, J., Ekre, R., Emerson, H., Phillips, N., Zhong, L., Smith, G., Mabrouki, R., Swanberg, D., 2022. Field-Scale

Lysimeter Studies of Glass and Cementitious Waste Forms at the Hanford Site. Proc Waste Manag Phoenix, AZ 22442.
[134] Pierce, E.M., Rodriguez, E.A., Calligan, L.J., Shaw, W.J., McGrail, B.P., 2008. An experimental study of the dissolution rates of simulated aluminoborosilicate waste glasses as a function of pH and temperature under dilute conditions. Appl Geochem 23, 2559–2573. https://doi.org/10.1016/j.apgeochem.2008.05.006.
[135] Vienna, J., Neeway, J., Kerisit, S., Ryan, J., 2018. Impacts of glass composition, pH, and temperature on glass forward dissolution rate. npj Mater Degrad 2, 1–12. https://doi.org/10.1038/s41529-018-0042-5.
[136] Bibler, N., Jurgensen, A., 1987. Leaching Tc-99 from SRP Glass in Simulated Tuff and Salt Groundwaters. DP-MS-87-70. Savannah River Laboratory, Aiken, SC.
[137] Reiser, J.T., Neeway, J.J., Parruzot, B.P., Cordova, E.A., Cooley, S.K., Vienna, J. D., 2023. Product Consistency Test and Vapor Hydration Test Comparisons of a Radioactive Hanford Waste Glass with Its Non-Radioactive Simulant Glass. PNNL-34123. Pacific Northwest National Laboratory, Richland, WA.
[138] Pierce, E., McGrail, B., Valenta, M., Strachan, D., 2006. The ACcelerated Weathering of A Radioactive Low-activity Waste Glass under Hydraulically Unsaturated Conditions: Experimental Results from A Pressurized Unsaturated Flow Test. Nucl Technol 155, 149–165.
[139] Gin, S., Jollivet, P., Tribet, M., Peuget, S., Schuller, S., 2017. Radionuclides containment in nuclear glasses: an overview. Radiochim Acta 105, 927–959. https://doi.org/10.1515/ract-2016-2658.
[140] Gin, S., Delaye, J.-M., Angeli, F., Schuller, S., 2021. Aqueous alteration of silicate glass: state of knowledge and perspectives. njp Mater Degrad 5, 42. https://doi.org/10.1038/s41529-021-00190-5.
[141] Ribet, S., Muller, I., Pegg, I., Gin, S., Frugier, P., 2004. Compositional Effects on the Long-Term Durability of Nuclear Waste Glasses: A Statistical Approach. In: Proc. of Mater. Res. Soc, 824, pp. 240–245.
[142] Fournier, M., Gin, S., Frugier, P., 2014. Resumption of nuclear glass alteration: state of the art. J Nucl Mater 448, 348–363. https://doi.org/10.1016/j.jnucmat.2014.02.022.
[143] Crum, J.V., Reiser, J.T., Parruzot, B.P., Neeway, J.J., Bonnett, J.F., Kerisit, S.N., Cooley, S.K., Ryan, J.V., Smith, G.L., Asmussen, R.M., 2021. Seeded Stage III glass dissolution behavior of a statistically designed glass matrix. J Am Ceram Soc 104, 4145–4162. https://doi.org/10.1111/jace.17823.
[144] Ebert, W.L., Bates, J.K., Bourcier, W.L., 1991. The hydration of borosilicate waste glass in liquid water and steam at 200 °C. Waste Manag 11, 205–221. https://doi.org/10.1016/0956-053X(91)90068-G.
[145] P. Van Iseghem, B. Grambow, The long-term corrosion and modelling of two simulated Belgian reference high-level waste glasses, pp. 631–639, Proc. of Mater. Res. Soc., 112. Edited by M. J. Apted and R. E. Westerman, 1987.
[146] Fournier, M., Gin, S., Frugier, P., Mercado-Depierre, S., 2017. Contribution of zeolite-seeded experiments to the understanding of resumption of glass alteration. npj Mater Degrad 1, 17. https://doi.org/10.1038/s41529-017-0018-x.
[147] L.L. Hench, J. Hutchins, S. Weiderhorn, A. Cooper, D. Readey, F. VerSnyder, R. Ewing, R. Staehle, DOE/TIC-11219, Alternative Waste Form Peer Review Panel. The Evaluation and Review of Alternative Waste Forms for Immobilization of High-level Radioactive Wastes. Report number 2, U.S. DOE, 1980.
[148] L.L. Hench, J. Hutchins, S. Weiderhorn, A. Cooper, D. Readey, F. VerSnyder, R. Ewing, R. Staehle, DOE/TIC-1 1612, Interface Working Group on High-Level Waste Form Selection Factors. A Method for Product Performance Evaluation of Candidate Waste Forms for Immobilization of High-level Radioactive Wastes, U.S. DOE, 1982.
[149] Thorpe, C.L., Neeway, J.J., Pearce, C.I., Hand, R.J., Fisher, A.J., Walling, S.A., Hyatt, N.C., Kruger, A.A., Schweiger, M., Kosson, D.S., Arendt, C.L., Marcial, J., Corkhill, C.L., 2021. Forty years of durability assessment of nuclear waste glass by standard methods. npj Mater Degrad 5, 61. https://doi.org/10.1038/s41529-021-00210-4.
[150] WRPS, 2016. Integrated Disposal Facility Model Package Report: ILAW Glass Release. RPP-RPT-59341. Rev. 0A. Washington River Protection Solutions, Richland, WA.
[151] Freedman, V., Ryan, J., Bacon, D., 2015. Immobilized Low-Activity Waste Glass Release Data Package for the Integrated Disposal Facility Performance Assessment. PNNL-24615. Pacific Northwest National Laboratory, Richland, WA.
[152] ASTM C1285-21, Standard Test Methods for Determining the Chemical Durability of Nuclear Waste Glasses: The Product Consistency Test (PCT), American Society for Testing and Materials International, 2021.
[153] Zapol, P., He, H., Kwon, K., Criscenti, L., 2013. First-principles study of hydrolysis reaction barriers in a sodium borosilicate glass. Int J Appl Glass Sci 4, 395–407. https://doi.org/10.1111/Ijag.12052.
[154] Ford, D., He, H., Zapol, P., 2015. Density Functional Theory Calculations of Hydrolysis Reactions on a Sodium Borosilicate Glass Surface. FCRD-MRWFD-2015-000149. Argonne National Laboratory, Lemont, IL.
[155] Zapol, P., 2014. Reaction Barriers for Glass Corrosion from First Principles Calculations. FCRD-UFD-2014-000310. Argonne National Laboratory, Lemont, IL.
[156] Hrma, P., Piepel, G., Schweiger, M., Smith, D., Kim, D.-S., Redgate, P., Vienna, J., Lopresti, C., Simpson, D., Peeler, D., Langowski, M., 1994. Property/Composition Relationships for Hanford High-Level Waste Glasses Melting at 1150°C. PNL-10359. Pacific Northwest Laboratory, Richland, WA.
[157] Debure, M., De Windt, L., Frugier, P., Gin, S., 2013. HLW glass dissolution in the presence of magnesium carbonate: diffusion cell experiment and coupled modeling of diffusion and geochemical interactions. J Nucl Mater 443, 507–521. https://doi.org/10.1016/j.jnucmat.2013.07.068.
[158] Aréna, H., Rébiscoul, D., Garcès, E., Godon, N., 2019. Comparative effect of alkaline elements and calcium on alteration of International Simple Glass. npj Mater Degrad 3, 1–10. https://doi.org/10.1038/s41529-019-0072-7.
[159] Mercado-Depierre, S., Angeli, F., Frizon, F., Gin, S., 2013. Antagonist effects of calcium on borosilicate glass alteration. J Nucl Mater 441, 402–410. https://doi.org/10.1016/j.jnucmat.2013.06.023.
[160] Utton, C.A., Hand, R.J., Bingham, P.A., Hyatt, N.C., Swanton, S.W., Williams, S.J., 2013. Dissolution of vitrified wastes in a high-pH calcium-rich solution. J Nucl Mater 435, 112–122. https://doi.org/10.1016/j.jnucmat.2012.12.032.
[161] J.J. Neeway, 2023. Effect of composition on the corrosion behavior of 24 statistically designed alkali-borosilicate waste glasses, submitted to J. Nucl. Mater.
[162] ASTM C1663–18, Standard Test Method for Measuring Waste Glass or Glass Ceramic Durability by Vapor Hydration Test, American Society for Testing and Materials International, 2021.
[163] Jiricka, A., Vienna, J., Hrma, P., Strachan, D., 2001. The effect of experimental conditions and evaluation techniques on the alteration of low activity glasses by vapor hydration. J Non-Cryst Solids 292, 25–43. https://doi.org/10.1016/S0022-3093(01)00875-4.
[164] Vienna, J., Jiricka, A., Hrma, P., Smith, D., Lorier, T., Schulz, R., Reamer, I., 2001. Hanford Immobilized LAW Product Acceptance Testing: Tanks Focus Area Results. PNNL-13744. Pacific Northwest National Laboratory, Richland, WA.
[165] Neeway, J.J., Parruzot, B.P., Bonnett, J.F., Reiser, J.T., Kerisit, S.N., Ryan, J.V., Crum, J.V., 2020. Acceleration of glass alteration rates induced by zeolite seeds at controlled pH. Appl Geochem 113, 104515. https://doi.org/10.1016/j.apgeochem.2019.104515.
[166] M. Bauchy, Stability temperature region for zeolites in glass corrosion solutions vs pH, personal correspondence, 2023.
[167] Zhen-Wu, B.Y., Prentice, D.P., Simonetti, D., Ryan, J.V., Sant, G., Bauchy, M., 2021. Predicting zeolites' stability during the corrosion of nuclear waste immobilization glasses: Comparison with glass corrosion experiments. J Nucl Mater 547, 152813. https://doi.org/10.1016/j.jnucmat.2021.152813.
[168] Bacon, D., Meyer, P., Neeway, J.J., Fang, Y., Asmussen, R.M., Strickland, C., 2018. Field-Scale Lysimeter Studies of Low-Activity Waste Form Degradation: Implementation Plan. RPT-IGTP-017 Rev 0.0, PNNL-27394. Pacific Northwest National Laboratory, Richland, WA.
[169] Muller, I., Joseph, I., Perez-Cardenas, F., Pegg, I., 2008. LAW Glass Testing and VHT model assessment. VSL-08R1410-1. Vitreous State Laboratory at the Catholic University of America, Washington, D.C.
[170] Narayanasamy, S., Jollivet, P., Godon, N., Angeli, F., Gin, S., Cabié, M., Cambedouzou, J., Le Guillou, C., Abdelouas, A., 2019. Influence of composition of nuclear waste glasses on vapor phase hydration. J Nucl Mater 525, 53–71. https://doi.org/10.1016/j.jnucmat.2019.07.015.
[171] Petkus, L., 2003. Low Act Contain Cent Cool Data, Pers Corresp 074181.
[172] Jantzen, C.M., Bickford, D.E., 1984. Leaching of devitrified glass containing simulated SRP nuclear waste. Proc Mater Res Soc 44, 135–146.
[173] Riley, B., Hrma, P., Rosario, J., 2001. Impact of HLW Glass Crystallinity on the PCT Response. PNNL-13491. Pacific Northwest National Laboratory, Richland, WA.
[174] D. Kim, D. Peeler, P. Hrma, Effect of Crystallization on the Chemical Durability of Simulated Nuclear Waste Glasses, pp. 177–185, Proc. of Ceram. Trans., 61, 1995.
[175] Kroll, J., Vienna, J., Schweiger, M., 2016. Effects of Al_2O_3, B_2O_3, Li_2O, Na_2O, and SiO_2 on nepheline crystallization in hanford high level waste glasses. Proc Ceram Trans 260.
[176] Vienna, J., Kroll, J., Hrma, P., Lang, J., Crum, J., 2017. Submixture model to predict nepheline precipitation in waste glasses. Int J Appl Glass Sci 8, 143–157. https://doi.org/10.1111/ijag.12207.
[177] Lonergan, C., Kim, D., Vienna, J., 2021. Crystallization Constraints for WTP LAW Operations: Assessment of CCC Impacts on VHT and PCT. PNNL-31138. Pacific Northwest National Laboratory, Richland, WA.
[178] Jantzen, C.M., Pickett, J.B., Brown, K.G., Edwards, T.B., Beam, D.C., 1995. Process/Product models for the defense waste processing facility (DWPF): Part I: Predicting glass durability from composition using a Thermodynamic Hydration Energy Reaction Model (THERMO). WSRC-TR-93-672. Westinghouse Savannah River Company, Aiken, SC.
[179] Taylor, P., Campbell, A.B., Owen, D.G., 1983. Liquid immiscibility in the systems X_2O-MO-B_2O_3-SiO_2 (X=Na, K; M=Mg, Ca, Ba) and Na_2O-MgO-BaO-B_2O_3-SiO_2. J Am Ceram Soc 66, 347–351. https://doi.org/10.1111/j.1151-2916.1983.tb10046.x.
[180] D. Peeler, P. Hrma, Predicting liquid immiscibility in multicomponent nuclear waste glasses, pp. 219–222, PNL-SA-23488; CONF-940416–940417, Proc. of Ceram. Trans., 45, 1994.
[181] T.B. Edwards. 2002. SME Acceptability Determination for DWPF Process Control. WSRC-TR-95–000364, Rev. 4. Savannah River Site, Aiken, SC.
[182] Reiser, J.T., Lu, X., Parruzot, B., Liu, H., Subramani, T., Kaya, H., Kissinger, R.M., Crum, J.V., Ryan, J.V., Navrotsky, A., Kim, S.H., Vienna, J.D., 2021. Effects of Al:Si and (Al + Na):Si ratios on the properties of the international simple glass, part I: physical properties. J Am Ceram Soc 104, 167–182. https://doi.org/10.1111/jace.17449.
[183] EPA, Land Disposal Restrictions 40 CFR 268, Washington, D.C., 2006.
[184] Kot, W., Klatt, K., Muller, I., Wilson, C., Pegg, I., Bates, D., Piepel, G., Weier, D., 2003. Regulatory spike testing of RPP-WTP LAW and HLW glasses for compliance with land disposal restrictions. VSL-03R3760-1. The Catholic University of America, Washington, D.C.
[185] Henckel, K., 2017. Land Disposal Restriction Treatability Variance Petition for Hanford Tank Waste. 24590-WTP-RPT-ENV-03-003, Rev. 2. River Protection Project, Hanford Tank Waste Treatment and Immobilization Plant, Richland, WA.
[186] Schleif, S., 2019. Approval of land disposal restriction treatability variance petition for hanford tank waste, personal correspondence. CCN 317076.

[187] Volf, M., 1984. Chemical Approach to Glass. Glass Science and Technology. 978-0444996350. Elsevier,, New York, NY.
[188] Vienna, J.D., Hrma, P., Crum, J.V., Mika, M., 2001. Liquidus temperature–composition model for multi-component glasses in the Fe, Cr, Ni, and Mn spinel primary phase field. J. Non-cryst. Solids 292, 1–24. https://doi.org/10.1016/S0022-3093(01)00874-2.
[189] C. Jantzen, First principles process-product models for vitrification of nuclear waste: Relationship of glass composition to glass viscosity, resistivity, liquidus temperature, and durability, pp. 37–51, Proc. of Ceram. Trans., 23. Westerville, OH, 1991.
[190] Du, J., Lu, X., Gin, S., Delaye, J.-M., Deng, L., Taron, M., Bisbrouck, N., Bauchy, M., Vienna, J.D., 2021. Predicting the dissolution rate of borosilicate glasses using QSPR analysis based on molecular dynamics simulations. J Am Ceram Soc 104, 4445–4458. https://doi.org/10.1111/jace.17857.
[191] Lu, X., Du, J., 2020. Quantitative structure-property relationship (QSPR) analysis of calcium aluminosilicate glasses based on molecular dynamics simulations. J Non-Cryst Solids 530, 119772. https://doi.org/10.1016/j.jnoncrysol.2019.119772.
[192] Yu, Y., Wang, B., Wang, M., Sant, G., Bauchy, M., 2016. Revisiting silica with ReaxFF: towards improved predictions of glass structure and properties via reactive molecular dynamics. J Non-Cryst Solids 443, 148–154. https://doi.org/10.1016/j.jnoncrysol.2016.03.026.
[193] Kapoor, S., Semitela, Â., Goel, A., Xiang, Y., Du, J., Lourenço, A.H., Sousa, D.M., Granja, P.L., Ferreira, J.M.F., 2015. Understanding the composition–structure–bioactivity relationships in diopside ($CaO{\cdot}MgO{\cdot}2SiO_2$)–tricalcium phosphate ($3CaO{\cdot}P_2O_5$) glass system. Acta Biomater 15, 210–226. https://doi.org/10.1016/j.actbio.2015.01.001.
[194] Deng, L., Du, J., 2018. Effects of system size and cooling rate on the structure and properties of sodium borosilicate glasses from molecular dynamics simulations. J Chem Phys 148, 024504. https://doi.org/10.1063/1.5007083.
[195] Lu, X., Deng, L., Gin, S., Du, J., 2019. Quantitative structure-property relationship (QSPR) analysis of ZrO_2-containing soda-lime borosilicate glasses. J Phys Chem B 123, 1412–1422. https://doi.org/10.1021/acs.jpcb.8b11108.
[196] Lu, X., Reiser, J.T., Parruzot, B., Deng, L., Gussev, I.M., Neuefeind, J.C., Graham, T.R., Liu, H., Ryan, J.V., Kim, S.H., Washton, N., Lang, M., Du, J., Vienna, J.D., 2021. Effects of Al:Si and (Al + Na):Si ratios on the properties of the international simple glass, part II: Structure. J Am Ceram Soc 104, 183–207. https://doi.org/10.1111/jace.17447.
[197] Gunnell, L.L., Manwaring, K., Lu, X., Reynolds, J., Vienna, J., Hedengren, J., 2022. Machine learning with gradient-based optimization of nuclear waste vitrification with uncertainties and constraints. Processes 10, 2365. https://doi.org/10.3390/pr10112365.
[198] Kerisit, S.N., Cooley, S.K., Asmussen, R.M., Smith, G.L., 2022. Immobilized Low-Activity Waste Glass Corrosion Model: Parameterization, Evaluation, and Composition Dependence of the Ion-Exchange Rate Model Term. PNNL-33157. Pacific Northwest National Laboratory, Richland, WA.
[199] Lonergan, C., Neeway, J., 2017. A Critical Review of Ion Exchange in Nuclear Waste Glasses to Support the Immobilized Low-Activity Waste Integrated Disposal Facility Rate Model. PNNL-26594. Pacific Northwest National Laboratory, Richland, WA.
[200] Parruzot, B., Crum, J.V., Reiser, J.T., Neeway, J.J., Kerisit, S.N., Daniel, R.C., Bonnett, J.F., Reyes, R.A., Seymour, L.M., Burns, C.A., Ryan, J.V., Smith, G.L., Asmussen, R.M., 2022. Effect of zeolite type, temperature, and pH on Stage III glass alteration behavior for two nuclear waste glasses. J Nucl Mater 567, 153717. https://doi.org/10.1016/j.jnucmat.2022.153717.
[201] Crum, J., Parruzot, B., Kerisit, S., Cooley, S., Song, X., Fang, Y., Ryan, J., Neeway, J., Bonnett, J., Daniel, R., Seymour, L., Reiser, J., Reyes, R., Burns, C., Smith, G., Asmussen, R., 2022. FY2022 Report: ILAW Glass Stage II and III Static Dissolution Testing and Modeling. PNNL 31758, Rev 1. Pacific Northwest National Laboratory,, Richland, WA.
[202] Ryan, J., Kerisit, S., Parruzot, B., Reiser, J., Lumetta, N., Cooley, S., Schonewill, P., Bonnett, J., Cordova, E., Seymour, L., Asmussen, R., Smith, G., 2021. Stirred-Reactor Coupon Analysis: Determination of Glass Composition Effects on Forward-Rate Model Parameters. RPT-IGTP-024. Pacific Northwest National Laboratory, Richland, WA.
[203] Neeway, J.J., Rieke, P.C., Parruzot, B.P., Ryan, J.V., Asmussen, R.M., 2018. The dissolution behavior of borosilicate glasses in far-from equilibrium conditions. Geochim Cosmochim Acta 226, 132–148. https://doi.org/10.1016/j.gca.2018.02.001.
[204] EPA, SW-846 (method 1313), SW-846 - Validated Test Method 1313: Liquid Solid Partitioning as a Function of Extract pH Using a Parallel Batch Extraction Procedure, Environmental Protection Agency, 2017.
[205] J. Marcial, L. Nava-Farias, M.J. Schweiger, J.J. Neeway, C.I. Pearce, C. Arendt, D. K. Peeler, S. Walling, C.L. Thorpe, C.L. Corkhill, R.J. Hand, D.S. Kosson, R. Delapp, A.A. Kruger, Evaluating an EPA leaching test (Method 1313) to relate the long-term performance of nuclear waste glasses and ancient glasses pp. 21243, Proc. of Waste Management, 2021.
[206] Neeway, J.J., Pierce, E.M., Freedman, V.L., Ryan, J.V., Qafoku, N.P., 2014. A Strategy to Conduct an Analysis of the Long-Term Performance of Low-Activity Waste Glass in a Shallow Subsurface Disposal System at Hanford. PNNL-23503. Pacific Northwest National Laboratory, Richland, WA.
[207] Gervasio, V., Vienna, J., Cooley, S., Baird, S., Bellofatto, D., Westman, B., Kim, D., Lu, X., Lang, J., Cutforth, D., Rivers, E., Lumetta, N., 2022. Experimental Verification of the Preliminary Enhanced LAW Glass Formulation Algorithm. PNNL-33233. Pacific Northwest National Laboratory, Richland, WA.
[208] Gervasio, V., Vienna, J., Lang, J., Westman, B., Sannoh, S., Russell, R., Kim, D., Cooley, S., George, J., Cutforth, D., Baird, S., 2021. Enhanced Hanford Low-Activity Waste Glass Property Data Development: Phase 4. PNNL-31556. Pacific Northwest National Laboratory, Richland, WA.
[209] Lonergan, C., George, J., Cutforth, D., Jin, T., Cholsaipant, P., Sannoh, S., Skidmore, C., Stanfill, B., Cooley, S., Piepel, G., Russell, R., Vienna, J., 2019. Enhanced Hanford Low-Activity Waste Glass Property Data Development: Phase 3. PNNL-29847. Pacific Northwest National Laboratory,, Richland, WA.
[210] Russell, R., Mccarthy, B., Cooley, S., Piepel, G., Cordova, E., Sannoh, S., Gervasio, V., Schweiger, M., Lang, J., Skidmore, C., Lonergan, C., Stanfill, B., Meline, J., Vienna, J., 2019. Enhanced Hanford Low-Activity Waste Glass Property Data Development: Phase 2. PNNL-28838, Rev. 1. Pacific Northwest National Laboratory, Richland, WA.
[211] Russell, R., Jin, T., Mccarthy, B., Darnell, L., Rinehart, D., Bonham, C., Gervasio, V., Mayer, J., Arendt, C., Lang, J., Schweiger, M., Vienna, J., 2017. Enhanced Hanford Low-Activity Waste Glass Property Data Development: Phase I. PNNL-26630. Pacific Northwest National Laboratory, Richland, WA.
[212] Gervasio, V., Neeway, J., Vienna, J., Lang, J., Westman, B., Reiser, J., Lonergan, C., Lu, X., Baird, S., Cutforth, D., Peterson, M., 2023. Enhanced Hanford Low-Activity Waste Glass Property Data Development: Phase 5 and Phase 6. PNNL-DRAFT. Pacific Northwest National Laboratory, Richland, WA.
[213] Antono, E., Matsuzawa, N.N., Ling, J., Saal, J.E., Arai, H., Sasago, M., Fujii, E., 2020. Machine-learning guided quantum chemical and molecular dynamics calculations to design novel hole-conducting organic materials. J Phys Chem A 124, 8330–8340. https://doi.org/10.1021/acs.jpca.0c05769.
[214] Lu, X., Ren, M., Deng, L., Benmore, C.J., Du, J., 2019. Structural features of ISG borosilicate nuclear waste glasses revealed from high-energy X-ray diffraction and molecular dynamics simulations. J Nucl Mater 515, 284–293. https://doi.org/10.1016/j.jnucmat.2018.12.041.
[215] Lu, X., Deng, L., Du, J., 2018. Effect of ZrO_2 on the structure and properties of soda-lime silicate glasses from molecular dynamics simulations. J Non-Cryst Solids 491, 141–150. https://doi.org/10.1016/j.jnoncrysol.2018.04.013.
[216] Ren, M., Deng, L., Du, J., 2017. Surface structures of sodium borosilicate glasses from molecular dynamics simulations. J Am Ceram Soc 100, 2516–2524. https://doi.org/10.1111/jace.14654.
[217] Yeon, J., van Duin, A.C.T., 2016. ReaxFF Molecular Dynamics Simulations of Hydroxylation Kinetics for Amorphous and Nano-Silica Structure, and Its Relations with Atomic Strain Energy. J Phys Chem C 120, 305–317. https://doi.org/10.1021/acs.jpcc.5b09784.
[218] Rimsza, J.M., Deng, L., Du, J., 2016. Molecular dynamics simulations of nanoporous organosilicate glasses using Reactive Force Field (ReaxFF). J Non-Cryst Solids 431, 103–111. https://doi.org/10.1016/j.jnoncrysol.2015.04.031.
[219] Deng, L., Du, J., 2016. Development of effective empirical potentials for molecular dynamics simulations of the structures and properties of boroaluminosilicate glasses. J Non-Cryst Solids 453, 177–194. https://doi.org/10.1016/j.jnoncrysol.2016.09.021.
[220] Lu, X., Sargin, I., Vienna, J.D., 2021. Predicting nepheline precipitation in waste glasses using ternary submixture model and machine learning. J Am Ceram Soc 104, 5636–5647. https://doi.org/10.1111/jace.17983.
[221] Lu, X., Deng, L., Du, J., Vienna, J.D., 2021. Predicting boron coordination in multicomponent borate and borosilicate glasses using analytical models and machine learning. J Non-Cryst Solids 553, 120490. https://doi.org/10.1016/j.jnoncrysol.2020.120490.
[222] Liu, H., Fu, Z., Yang, K., Xu, X., Bauchy, M., 2021. Machine learning for glass science and engineering: a review. J Non-Cryst Solids 557, 119419. https://doi.org/10.1016/j.jnoncrysol.2019.04.039.
[223] Anoop Krishnan, N.M., Mangalathu, S., Smedskjaer, M.M., Tandia, A., Burton, H., Bauchy, M., 2018. Predicting the dissolution kinetics of silicate glasses using machine learning. J Non-Cryst Solids 487, 37–45. https://doi.org/10.1016/j.jnoncrysol.2018.02.023.
[224] Abboud, A.W., Guillen, D.P., Hrma, P., Kruger, A.A., Klouzek, J., Pokorny, R., 2021. Heat transfer from glass melt to cold cap: computational fluid dynamics study of cavities beneath cold cap. Int J Appl Glass Sci 12, 233–244. https://doi.org/10.1111/ijag.15863.
[225] Ferkl, P., Hrma, P., Abboud, A., Guillen, D.P., Vernerová, M., Kloužek, J., Hall, M., Kruger, A.A., Pokorný, R., 2023. Conversion degree and heat transfer in the cold cap and their effect on glass production rate in an electric melter. Int J Appl Glass Sci 14, 318–329. https://doi.org/10.1111/ijag.16615.
[226] Hrma, P., Klouzek, J., Pokorny, R., Lee, S.M., Kruger, A.A., 2019. Heat transfer from glass melt to cold cap: gas evolution and foaming. J Am Ceram Soc 102, 5853–5865. https://doi.org/10.1111/jace.16484.
[227] Lee, S., Ferkl, P., Pokorny, R., Klouzek, J., Hrma, P., Eaton, W.C., Kruger, A.A., 2020. Simplified melting rate correlation for radioactive waste vitrification in electric furnaces. J Am Ceram Soc 103, 5573–5578. https://doi.org/10.1111/jace.17281.
[228] Marcial, J., Pokorný, R., Kloužek, J., Vernerová, M., Lee, S., Hrma, P., Kruger, A., 2021. Effect of water vapor and thermal history on nuclear waste feed conversion to glass. Int J Appl Glass Sci 12, 145–157. https://doi.org/10.1111/ijag.15803.
[229] Ferkl, P., Hrma, P., Abboud, A.W., Guillen, D.P., Vernerová, M., Kloužek, J., Marcial, J., Hall, M.A., Eaton, W.C., Kruger, A.A., Pokorný, R., 2023. Modeling Effects of Nuclear Waste Feed Properties on Glass Production Rate in Joule-Heated Melters. Proc Waste Manag 23555.
[230] Marcial, J., Luksic, S., Kloužek, J., Vernerová, M., Cutforth, D., Varga, T., Hrma, P., Kruger, A., Pokorný, R., 2022. In-situ X-ray and visual observation of foam morphology and behavior at the batch-melt interface during melting of

simulated waste glass. Ceram Int 48, 7975–7985. https://doi.org/10.1016/j.ceramint.2021.11.344.

[231] Luksic, S.A., Pokorny, R., Hrma, P., Varga, T., Rivers, E.L., Buchko, A.C., Klouzek, J., Kruger, A.A., 2021. Through a glass darkly: In-situ x-ray computed tomography imaging of feed melting in continuously fed laboratory-scale glass melter. Ceram Int 47, 15807–15818. https://doi.org/10.1016/j.ceramint.2021.02.153.

[232] Hujova, M., Pokorny, R., Klouzek, J., Dixon, D.R., Cutforth, D.A., Lee, S., McCarthy, B.P., Schweiger, M.J., Kruger, A.A., Hrma, P., 2017. Determination of heat conductivity of waste glass feed and its applicability for modeling the batch-to-glass conversion. J Am Ceram Soc 100, 5096–5106. https://doi.org/10.1111/jace.15052.